J Physiol 588.12 (2010) pp 2109–2132

The Journal of Physiology

Differences in subthreshold resonance of hippocampal pyramidal cells and interneurons: the role of h-current and passive membrane characteristics

Rita Zemankovics[1], Szabolcs Káli[1,2], Ole Paulsen[3,4], Tamás F. Freund[1,5] and Norbert Hájos[1]

[1] *Department of Cellular and Network Neurobiology, Institute of Experimental Medicine, Hungarian Academy of Sciences, Budapest, Hungary*
[2] *Infobionic and Neurobiological Plasticity Research Group, Hungarian Academy of Sciences–Péter Pázmány Catholic University–Semmelweis University, Budapest, Hungary*
[3] *Department of Physiology, Anatomy and Genetics, University of Oxford, Oxford, UK*
[4] *Department of Physiology, Development and Neuroscience, University of Cambridge, Cambridge, UK*
[5] *Faculty of Information Technology, Péter Pázmány Catholic University, Budapest, Hungary*

The intrinsic properties of distinct types of neuron play important roles in cortical network dynamics. One crucial determinant of neuronal behaviour is the cell's response to rhythmic subthreshold input, characterised by the input impedance, which can be determined by measuring the amplitude and phase of the membrane potential response to sinusoidal currents as a function of input frequency. In this study, we determined the impedance profiles of anatomically identified neurons in the CA1 region of the rat hippocampus (pyramidal cells as well as interneurons located in the stratum oriens, including OLM cells, fast-spiking perisomatic region-targeting interneurons and cells with axonal arbour in strata oriens and radiatum). The basic features of the impedance profiles, as well as the passive membrane characteristics and the properties of the sag in the voltage response to negative current steps, were cell-type specific. With the exception of fast-spiking interneurons, all cell types showed subthreshold resonance, albeit with distinct features. The HCN channel blocker ZD7288 (10 μM) eliminated the resonance and changed the shape of the impedance curves, indicating the involvement of the hyperpolarisation-activated cation current I_h. Whole-cell voltage-clamp recordings uncovered differences in the voltage-dependent activation and kinetics of I_h between different cell types. Biophysical modelling demonstrated that the cell-type specificity of the impedance profiles can be largely explained by the properties of I_h in combination with the passive membrane characteristics. We conclude that differences in I_h and passive membrane properties result in a cell-type-specific response to inputs at given frequencies, and may explain, at least in part, the differential involvement of distinct types of neuron in various network oscillations.

(Received 11 December 2009; accepted after revision 20 April 2010; first published online 26 April 2010)
Corresponding author N. Hájos: Department of Cellular and Network Neurobiology, Institute of Experimental Medicine, Hungarian Academy of Sciences, Szigony u. 43, Budapest, 1083 Hungary. Email: hajos@koki.hu

Abbreviations BIC, Bayesian information criterion; FFT, fast Fourier transform; FS PTI, fast spiking perisomatic region-targeting interneuron; HCN channel, hyperpolarisation-activated cyclic nucleotide-gated channel; I_h, h-current; MP, membrane potential; OLM, oriens-lacunosum-moleculare; O-R, oriens-radiatum; PC, pyramidal cell.

Introduction

Information processing in neural networks depends on the behaviour of individual neurons, which is governed by both intrinsic membrane properties and synaptic inputs. Intrinsic membrane properties arise from the interaction of passive membrane properties and active conductances, i.e. the operation of voltage-gated ion channels. These built-in membrane characteristics of a cell shape the amplitude and the temporal dynamics of the neuronal response, influence the integration of synaptic inputs, and contribute to controlling the precise timing of the action potential output (Magee, 1998; Magee, 1999; Richardson *et al.* 2003; McLelland & Paulsen, 2009). Moreover, the presence of active conductances can endow neurons with the capability of producing

DOI: 10.1113/jphysiol.2009.185975

intrinsic membrane potential oscillations and resonance at different frequencies (Hutcheon & Yarom, 2000). These frequency tuning properties enable the cells to respond preferentially to inputs at certain frequencies (Pike *et al.* 2000), and they can influence the precise spike timing of the cell relative to the ongoing network activity (Lengyel *et al.* 2005; Kwag & Paulsen, 2009; McLelland & Paulsen, 2009). As a net effect these features of the cells may play a significant role in setting network dynamics (Hutcheon & Yarom, 2000).

In the hippocampus pyramidal cells are known to express subthreshold resonance at frequencies within the theta range (4–7 Hz) (Leung & Yu, 1998; Pike *et al.* 2000; Hu *et al.* 2002; Narayanan & Johnston, 2007), which might contribute to their membrane potential oscillations *in vivo* (Ylinen *et al.* 1995; Kamondi *et al.* 1998) as well as to their discharge properties (Pike *et al.* 2000). Recent studies have revealed that subthreshold resonance in pyramidal cells is predominantly mediated by the hyperpolarisation-activated cyclic nucleotide-gated channels (HCN channels), which generate a non-selective cation current – termed I_h (Hu *et al.* 2002). In addition to having a key role in producing resonance in distinct types of neurons and its vital function in pacemaker activities as well as in network oscillations (Kocsis & Li, 2004), this conductance has been suggested to contribute to synaptic waveform normalization (Magee, 1999) and even to learning processes (Nolan *et al.* 2003).

In addition to pyramidal cells, cortical neuronal networks contain morphologically and functionally diverse populations of inhibitory interneurons (Freund & Buzsáki, 1996; Klausberger & Somogyi, 2008). It has been shown that some hippocampal interneurons also tend to show frequency tuning properties (Gloveli *et al.* 2005; Lawrence *et al.* 2006) and can also resonate at certain frequencies (Pike *et al.* 2000). However, it is still unclear which GABAergic cell types show resonance at which frequencies, and what cellular mechanisms are involved.

To understand how neuronal networks operate, detailed knowledge of the intrinsic properties of the cells that are embedded in them would appear necessary, serving as a basis for realistic modelling. Therefore, we investigated the impedance profiles of distinct types of anatomically identified neurons in the CA1 region of rat hippocampal slices. We focused on the dissimilarities in the voltage response of the cells to sinusoidal current inputs and wanted to determine the role of I_h in producing these differences. Experimental data and computational modelling indicated that impedance characteristics are cell-type dependent, and that the impedance profiles of the cells were predominantly determined by the kinetic properties of I_h in combination with the passive membrane properties of the neurons.

Methods

Slice preparation

Animals were kept and used according to the regulations of the European Community's Council Directive of 24 November 1986 (86/609/EEC), and experimental procedures were reviewed and approved by the Animal Welfare Committee of the Institute of Experimental Medicine. Altogether 52 animals were used in this study and all the experiments comply with the policies and regulations of *The Journal of Physiology* given by Drummond (2009). Male Wistar rats (postnatal day 14–26) were decapitated under deep isoflurane anaesthesia, and their brains were removed into ice cold cutting solution (containing in mM: 252 sucrose, 2.5 KCl, 26 $NaHCO_3$, 0.5 $CaCl_2$, 5 $MgCl_2$, 1.25 NaH_2PO_4, 10 glucose, saturated with 95% O_2–5% CO_2). Horizontal hippocampal slices (400 μm) were cut using a vibrating blade microtome (Leica VT1000S). The slices were kept in an interface chamber containing artificial cerebrospinal fluid (ACSF) at room temperature for at least 1 h before use. The ACSF had the following composition (in mM): 126 NaCl, 2.5 KCl, 26 $NaHCO_3$, 2 $CaCl_2$, 2 $MgCl_2$, 1.25 NaH_2PO_4, 10 glucose, saturated with 95% O_2–5% CO_2. During the recordings the slices were kept submerged in a chamber perfused with ACSF at a flow rate of 3–4 ml min^{-1}. All recordings were made at 34–37°C.

Electrophysiological recordings and data analysis

Whole-cell patch-clamp experiments were performed under visual guidance using a Versascope (E. Marton Electronics, Canoga Park, CA, USA) or an infrared differential interference contrast microscope (Olympus BX61WI). Electrodes were pulled from borosilicate glass capillaries (Hilgenberg, Malsfeld, Germany). Pipette resistances were 3–5 MΩ when filled with the intrapipette solution. The intrapipette solution contained (in mM): 125 potassium gluconate, 6 KCl, 4 NaCl, 10 Hepes, 10 disodium creatine phosphate, 4 Mg-ATP, 0.3 Tris-GTP (pH 7.38; 284–290 mosmol l^{-1}). Biocytin at 5 mg ml^{-1} was added to the pipette solution for later morphological identification of the recorded cells. Recordings were made using an Axopatch 200B or a Multiclamp 700B amplifier (Molecular Devices, Sunnyvale, CA, USA). Data were digitised using a PCI-MIO-16-4E board (National Instruments, Austin, TX, USA). Traces were filtered at 2 kHz and digitised at 8 kHz in the current-clamp experiments and 6 kHz in the voltage-clamp experiments. Data for current-clamp experiments were acquired and analysed with Igor Pro 4.0 software (WaveMetrics, Inc., Lake Oswego, OR, USA). For voltage-clamp experiments data acquisition was carried out using the EVAN program (courtesy of Prof. I. Mody; UCLA, CA, USA) or Stimulog

software (courtesy of Prof. Z. Nusser; Institute of Experimental Medicine, Hungarian Academy of Sciences, Budapest, Hungary), and analysed with Origin 7.0 software (OriginLab Corp. Northamton, MA, USA).

The extracellular solution for current-clamp experiments was ACSF as described above. In all voltage-clamp experiments 50–100 μM picrotoxin and 2–3 mM kynurenic acid (Sigma-Aldrich, St Louis, MO, USA) were added to abolish synaptic events, and 0.5 μM TTX (Alomone Labs, Jerusalem, Israel) was added to block voltage-dependent Na^+ channels. Blocking the h-current was accomplished by adding 10 μM ZD7288 (4-ethylphenylamino-1,2-dimethyl-6-methylaminopyrimidinium chloride, Tocris Bioscience Ltd, Bristol, UK) to the bath solution. In voltage-clamp experiments, series resistance was compensated and was between 5 and 15 MΩ. Only cells with stable resting membrane potential and overshooting action potentials with stable amplitude were included in the study. Resting membrane potential was measured in bridge mode ($I = 0$) immediately after obtaining whole-cell access. Reported values for membrane potential were not corrected for the liquid junction potential.

From perisomatic region-targeting interneurons only those cells were included in this study which could be identified unequivocally as fast-spiking interneurons based on their action potential phenotype. These cells were characterised by a fast-decaying afterhyperpolarisation (AHP) measured at 25% of the AHP amplitude (less than 3.2 ms) and by the small width of action potentials determined at half peak amplitude of the first and the last action potentials of the train (less than 0.5 ms; for 800 ms, 0.2 nA pulses) (Han, 1994; Pawelzik *et al.* 2002; Lien & Jonas, 2003). To validate that the classification is not sensitive to this particular choice of parameters, we also did principal component analysis on 20 different parameters related to the action potential phenotype and firing pattern of these cells, and, by choosing an appropriate threshold value for the first principal component, obtained identical results.

The basic physiological characteristics of the cells were determined from the voltage responses to a series of hyperpolarising and depolarising square current pulses of 800 ms duration and amplitudes between −200 and 200 pA, at 20 pA intervals from a holding potential of −60 mV. To estimate the membrane time constant and the total membrane capacitance at −60 mV, single exponential functions with a common decay time constant were fitted simultaneously to the voltage responses to the five smallest amplitude hyperpolarising current steps (−20 to −100 pA) between 5 and 37.5 ms after the onset of the pulse. The median value of the membrane capacitance estimated from these fits was used. In order to estimate the input resistance of the cell, double exponential functions were fitted to the voltage traces during the current step, and the minimum and steady-state voltage values were determined (this procedure also allowed us to characterise the voltage sag; see below). Estimated steady-state voltage responses were then plotted against current amplitude for the five smallest amplitude hyperpolarising current steps (−20 to −100 pA), and the input resistance at −60 mV was estimated from the slope of the linear regression through these points (Fig. 2*A*).

In many cells, a voltage sag was observed in response to a hyperpolarising current pulse. We characterised this voltage sag by fitting the difference of two exponential functions to the membrane potential during the pulse (see above). The sag responses were described quite accurately by this class of function; our choice of functional description was further motivated by the fact that the response of a simple model of I_h-containing neurons (the linearised I_h model, described below) can be calculated analytically, and also predicts a sag shaped as a difference of exponential functions. Fitting a continuous function to the data allowed us to robustly estimate the relative sag amplitude, defined as the ratio of two differences in membrane potential: the difference between the minimum voltage during the sag and the steady-state voltage later in the pulse, and the difference between the steady-state voltage and the membrane potential measured immediately after the beginning of the step (see Fig. 2*B*). We also determined the peak delay, defined as the time of the negative peak of the membrane potential relative to the beginning of the current pulse. Both the relative sag amplitude and the peak delay were calculated for the five largest amplitudes of the negative current steps (−120 to −200 pA), and their median values were used to characterise the sag in each cell.

Characterisation of neuronal impedance profiles and resonance properties

To determine the impedance profile and subthreshold resonance properties of each cell, 3 s-long sinusoidal currents were injected into the cells with a peak-to-peak amplitude of 120 pA at fixed frequencies (0.5, 1, 2, 3, 4, 5, 6, 7, 8, 9, 10, 15, 20, 40 Hz). This amplitude represented the optimal trade-off between linearity (which requires a small input) and signal-to-noise ratio (which is better for large signals). Since the neuronal impedance is in general voltage dependent, measurements were repeated at different subthreshold membrane potentials (−60, −70, −80, and in some cases at −90 mV). These baseline potentials were manually adjusted by direct current (DC) injection through the recording electrode. The complex impedance value (Z) at a given frequency (f) was determined by calculating the fast Fourier transform (FFT) of the voltage response and dividing the FFT component corresponding to the input frequency by the equivalent FFT component

of the input current. We found that 3 s-long sinusoidal currents allowed us to estimate both the amplitude and the phase of the voltage response at a high level of precision, even for the lowest reported frequencies (see Supplemental Material).

The magnitude of the impedance was plotted against input frequency to give the impedance magnitude profile. In order to facilitate the comparison of multiple impedance magnitude profiles, we characterised the impedance magnitude curves by four summary statistics. First, we measured the impedance value at the lowest input frequency (0.5 Hz), $Z_{(0.5\ \mathrm{Hz})}$. Cutoff frequency (f_{cutoff}) was defined as the input frequency at which the magnitude of the impedance first dipped below $\frac{1}{\sqrt{2}} \cdot Z_{(0.5\ \mathrm{Hz})}$ (this definition returns the classic cutoff frequency $\frac{1}{2\pi RC}$ for a passive linear cell, where $R \approx Z_{(0.5\ \mathrm{Hz})}$). Since many of our cells displayed a clear peak in the impedance magnitude profile at some nonzero frequency, we also defined the resonance magnitude (Q) as the impedance magnitude at the resonance peak (maximal impedance value) divided by the impedance magnitude at the lowest input frequency (0.5 Hz), i.e. $Q = Z_{\max}/Z_{(0.5\ \mathrm{Hz})}$ (Hutcheon *et al.* 1996*b*). Finally, the frequency of maximal impedance ($f_{\max}$) was determined as the frequency at which the maximum impedance magnitude value was detected. In those cells that showed no peak in their impedance profile ($Q = 1$), $f_{\max}$ is equal to 0.5 Hz.

The phase of the impedance (which equals the difference between the phases of the voltage and current oscillations) was also determined and plotted as a function of frequency to define the phase profile of the neuron. Since positive values of this quantity (i.e. the response leading the input) indicate a membrane with non-linear properties with potential computational significance (see Results and Discussion), following Narayanan & Johnston (2008) we defined Φ_{L} as the area under the positive part of the phase profile. This is a robust measure of the resonance properties of the membrane. Finally, we combined the magnitude and phase of the impedance to obtain the complex-valued impedance of the neuron. A plot of the complex impedance for all frequencies (i.e. a plot of the imaginary part of the impedance against the real part as frequency varies, known as a Nyquist plot) is a useful indicator of the basic properties of a system, and is widely used in engineering applications.

Characterisation of I_{h} in different cell types

In order to determine the properties of I_{h}, 800 ms-long voltage-clamp steps were given in −10 mV increments up to −120 mV from a holding potential of −40 mV. Since I_{h} has quite slow activation kinetics, rather long voltage steps are needed to activate the current fully at a given membrane potential. However, most of the interneurons proved to be sensitive to prolonged hyperpolarising pulses, and therefore we adjusted our protocol to have the shortest possible voltage step that still enabled us to measure the current. Nevertheless, we note that the shortness of the steps, in combination with the voltage-dependent kinetics of I_{h}, may cause some negative shift (up to a few mV) of the estimated activation curves.

I_{h} was obtained by subtracting the current traces before and after the application of 10 μM ZD7288, a specific blocker of HCN channels (Harris & Constanti, 1995). This current difference trace during the voltage step was used to determine the time constant(s) of I_{h} activation as well as the steady-state current, while the tail current recorded immediately after the end of the step was used to estimate the steady-state activation function. To determine the time constant(s) of I_{h} activation, either a single- or a double-exponential model was fitted to the difference current recorded from 20 ms after the beginning of the voltage step to the end of the step. The steady-state current was determined concurrently for all step potentials by fitting exponential functions with a common time constant to the current traces during the late phase (last 500 ms) of the voltage step. The I_{h} activation curve was calculated by fitting single exponential functions to the tail current between 2 and 20 ms after the end of the voltage step (the first 2 ms were excluded to ignore fast transients), and extrapolating back to the end of the step to determine the instantaneous tail current. We then plotted the tail current as a function of the step potential, and fitted a sigmoidal function:

$$I(V) = \frac{I_{\max}}{1 + \exp\left(-\left(V - V_{1/2}\right)/m\right)} \qquad (1)$$

where $I_{\max}$ is the asymptotic maximum of the sigmoid, $V_{1/2}$ is the potential of half-maximal I_{h} activation, and $\frac{1}{4m}$ is the slope of the activation function at $V_{1/2}$. The measured tail current values at each voltage were then divided by $I_{\max}$ to arrive at the activation function for each cell.

The I_{h} reversal potential for each cell type was calculated for a subset of our cells from the open-channel I–V relationship, which was obtained by the following protocol: I_{h} was activated with an 800 ms-long pulse to −120 mV and this was followed by steps to different test potentials (from −110 to −40 mV in +10 mV increments). The instantaneous I–V plot was constructed from the tail current amplitudes measured at each test potential in the same way as described above, and a straight line was fitted through the data points. The reversal potential of I_{h} was defined as the voltage at which the fitted line crossed the V axis.

Once the I_h reversal potential was known, the maximal conductance of I_h in each cell could be determined from the steady-state I–V relationship. Assuming a sigmoidal form for the activation function, the steady-state current can be written as:

$$I_{ss} = \bar{g}_h \frac{1}{1 + \exp\left(-\left(V - V_{1/2}\right)/m\right)} (V - E_h) \quad (2)$$

where $\bar{g}_h$ is the maximal I_h conductance, and E_h is the I_h reversal potential. Three parameters of this function ($\bar{g}_h$, $V_{1/2}$ and m) were optimised to fit the measured I–V relationship, resulting in an estimate of the maximal conductance value for each cell.

Statistical analyses

Since, in many cases, data were not normally distributed (according to a Lilliefors test), non-parametric statistical tests were used whenever possible. We employed Wilcoxon's signed rank test to compare medians from two groups. When comparing more than two groups, a Kruskal–Wallis test was used, often followed by *post hoc* comparisons based on average ranks using Tukey–Kramer critical values to account for multiple comparisons. However, in a few cases for which no appropriate non-parametric test has been established (such as in a three-way design, or a two-way design combining between- and within-subject factors), conventional parametric tests (such as ANOVA) were used. Summary statistics are also displayed in a form appropriate for non-Gaussian distributions, including box plots, which indicate the median of the data as well as its interquartile range, with whiskers showing the full range of the data, and extreme outliers (data points outside 2.5 times the interquartile range) marked by crosses outside the whiskers. The notch around the median value indicates a robust estimate of the confidence of the median, such that non-overlapping notches for two groups mean that the two medians are significantly different at the 5% level.

Comparisons of the goodness of fit between models with a different number of free parameters were performed using the Bayesian information criterion (BIC) (Bishop, 2006). The BIC attempts to compensate for the fact that better fits are more easily achieved with more complex models by penalising models according to the number of free parameters. For each model we calculate the quantity:

$$\mathrm{BIC} = n \ln\left(\frac{\mathrm{RSS}}{n}\right) + k \ln(n) \quad (3)$$

where RSS is the residual sum of squares for the model, n is the number of data points, and k is the number of free parameters. Then, out of two or more models of the same data set, the best model is the one for which the quantity defined by eqn (3) is the smallest.

Anatomical identification of the cells

The methods for anatomical identification have been described in detail in Gulyás *et al.* (1993). Briefly, the recorded cells were filled with biocytin during the recording. After the recording the slices were fixed in 4% paraformaldehyde in 0.1 M phosphate buffer (PB; pH 7.4) for at least 1 h, followed by washout with PB several times and incubation in 30% sucrose in 0.01 M PB for at least 2 h. Then slices were freeze-thawed three times above liquid nitrogen and treated with 1% H_2O_2 in PB for 15 min to reduce the endogenous peroxidase activity. Recorded cells were visualised using avidin-biotinylated horseradish peroxidase complex reaction (Vector Laboratories Inc., Burlingame, CA, USA) with nickel-intensified 3,3′-diaminobenzidine as chromogen giving a dark reaction product. After dehydration and embedding in Durcupan, representative neurons were reconstructed using a drawing tube.

Computational model

In an attempt to capture quantitatively the experimentally measured impedance profiles of single hippocampal neurons, single-compartment models of varying complexity were constructed and their parameters were optimised. The simplest model, which will be referred to as the passive model, contained only the membrane capacitance and a (voltage-independent) leak conductance. The temporal evolution of the membrane potential (V_m) in this model cell can be described by the following equation:

$$C\frac{\mathrm{d}V_m}{\mathrm{d}t} = g_l (E_l - V_m) + I_i \quad (4)$$

where C is the total capacitance of the neuron, g_l is the leak conductance, E_l is the reversal potential of the leak current, and I_i is the external current injection.

The second model (called the I_h model) also contained, in addition to the membrane capacitance and the leak conductance, a voltage-gated hyperpolarisation-activated conductance, which was described by a Hodgkin–Huxley-type formalism with a single gating variable, and whose parameters matched the properties of I_h in different cell types as determined in our experiments. This model is defined by the following set of equations:

$$C\frac{\mathrm{d}V_m}{\mathrm{d}t} = g_l (E_l - V_m) + \bar{g}_h m_h (E_h - V_m) + I_i \quad (5)$$

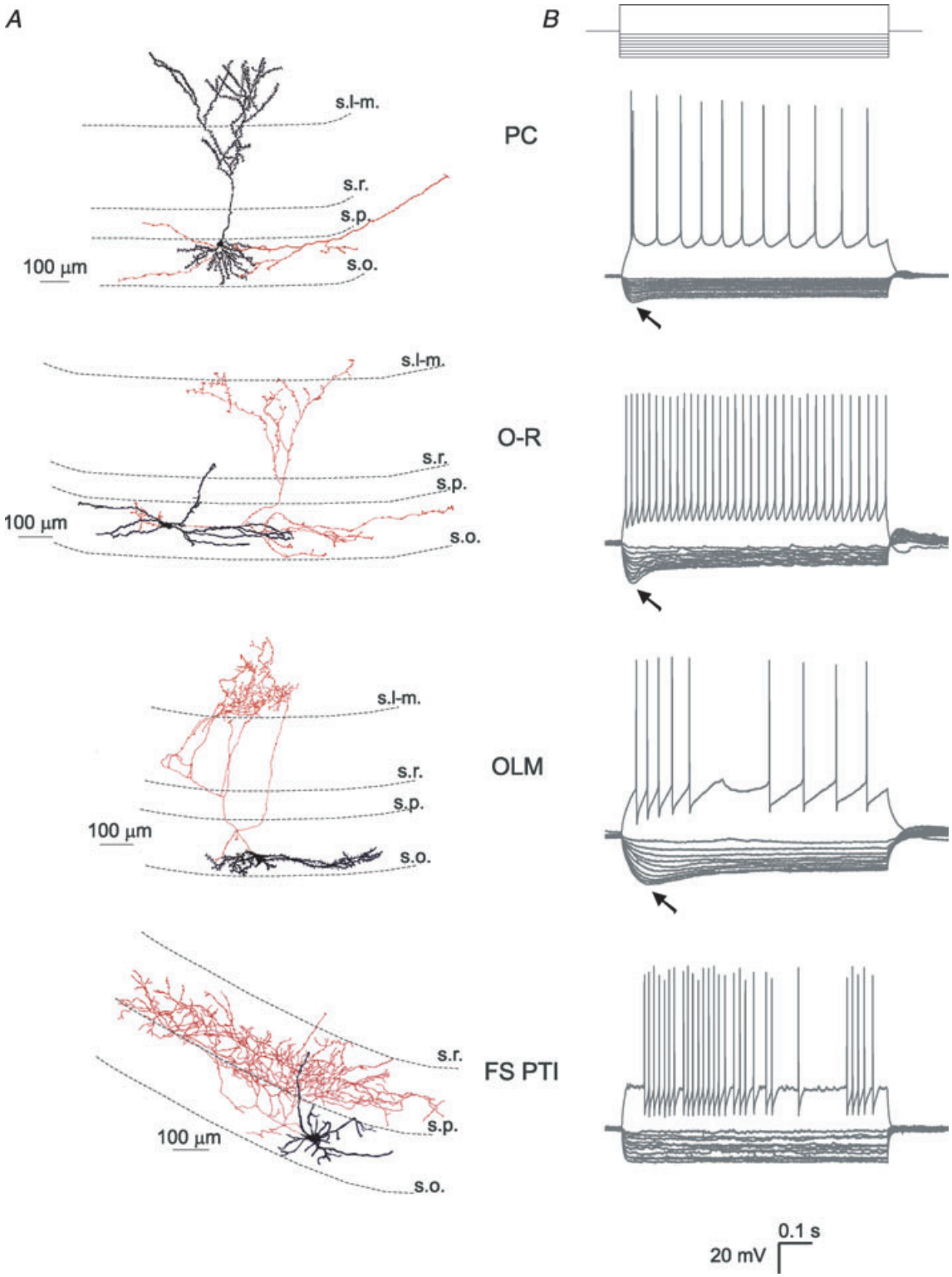

Figure 1. Light microscopic reconstructions and voltage responses to current steps of the investigated cell types recorded in the stratum oriens of hippocampal CA1 region
A, example artistic renderings of light microscopic reconstructions of a pyramidal cell (PC), an oriens-radiatum cell (O-R), an oriens-lacunosum-moleculare cell (OLM), and a fast spiking perisomatic region-targeting interneuron (FS PTI). Dendrites are represented in black and axons in red. Dendritic spines are enhanced for visibility. *B*, voltage responses to depolarising (200 pA) and hyperpolarising current steps (from −20 to −200 pA in increments of

Table 1. Passive membrane properties and sag characteristics of the investigated cell types

	PC ($n = 19$)	O-R ($n = 11$)	OLM ($n = 12$)	FS PTI ($n = 7$)
Input resistance (MΩ)	101 (91–131)	144 (116–199)	197 (169–211)	117 (112–219)
Membrane capacitance (pF)	155 (121–195)	97 (84–110)	181 (136–255)	106 (91–132)
Membrane time constant (ms)	16.6 (13.4–19.6)	18.5 (15.4–25.5)	37.7 (31.9–46.9)	8.7 (8.3–16.2)
Passive cutoff frequency (Hz)	9.6 (8.1–11.9)	8.6 (6.2–10.3)	4.2 (3.4–5.0)	18.4 (10.6–19.3)
Relative sag amplitude	0.175 (0.160–0.216)	0.687 (0.560–0.695)	0.445 (0.382–0.644)	0.074 (0.021–0.138)
Peak delay (ms)	44.7 (39.9–49.2)	36.8 (32.0–60.2)	92.3 (69.5–107.0)	74.0 (67.6–80.4)*

Data are presented as the median with interquartile range in parentheses. *$n = 2$ (only cells with a relative sag amplitude >0.1)

and

$$\frac{\mathrm{d}m_\mathrm{h}}{\mathrm{d}t} = \frac{m_\infty^{(h)}(V_\mathrm{m}) - m_\mathrm{h}}{\tau_\mathrm{h}(V_\mathrm{m})} \tag{6}$$

where $\bar{g}_\mathrm{h}$ is the maximal conductance of I_h, m_h is the gating variable for the activation of I_h, E_h is the I_h reversal potential, while $m_\infty^{(h)}(V_\mathrm{m})$ is the steady-state value and $\tau_\mathrm{h}(V_\mathrm{m})$ is the time constant for changes in m_h as a function of V_m.

For both of the above models, the impedance profile (the amplitude and phase of the voltage response to small-amplitude sinusoidal current injection as a function of input frequency) could be determined analytically by linearising all the defining equations in the vicinity of a given baseline potential. The explicit formulae derived in this manner allowed us to explore how the various parameters affect impedance, and vastly simplified the task of finding the optimal set of parameters to fit experimental data. Linearisation involved neglecting terms of second and higher order in the difference between the current membrane potential and the baseline potential in both the membrane voltage equation and the expressions for steady state activation of conductances, and neglecting the voltage dependence of the time constant of all voltage-gated conductances. The rationale for and further details of this procedure may be found in Hutcheon *et al.* (1994). For the passive model, this approach is exact (since the model is linear to begin with), and results in the following expression for the impedance of the membrane:

$$Z = \frac{1}{g_\mathrm{l} + i\omega C} \tag{7}$$

where $\omega = 2\pi f$, and f is the frequency of the oscillating input. Taking the absolute value of the complex impedance reproduces the well-known expression $|Z| = (g_\mathrm{l}^2 + \omega^2 C^2)^{-1/2}$ for the impedance magnitude.

In the I_h model, linearisation involved approximating the steady-state activation of I_h as $m_\infty^{(h)}(V_\mathrm{m}) \approx m_\infty^{(h)}(V_0) + b(V_\mathrm{m} - V_0)$ (where V_0 is the membrane potential in the absence of the oscillating input, b is the slope of the function $m_\infty^{(h)}(V_\mathrm{m})$ at V_0), and taking a voltage-independent value for τ_h. This allowed us to assume that, in response to a sinusoidal current injection, both V_m and m_h have a sinusoidal time dependence at the input frequency, and the amplitude and phase of these oscillations (relative to the input current) can be determined from eqns (5) and (6), producing the following formula for the (complex) impedance of the I_h model:

$$Z = \frac{1}{g_\mathrm{l} + i\omega C + \bar{g}_\mathrm{h} m_\infty^{(h)}(V_0) + \frac{\bar{g}_\mathrm{h} b(V_0 - E_\mathrm{h})}{1 + i\omega\tau_\mathrm{h}}} \tag{8}$$

Results

Using the whole-cell patch-clamp method, we recorded from hippocampal neurons located in the stratum oriens or pyramidale of the CA1 region. During the recording the cells were filled with biocytin and morphologically identified *post hoc* on the basis of their dendritic and axonal arborisation. In addition to pyramidal cells (PCs, $n = 27$, Fig. 1*A*), three interneuron types were recognized. Those interneurons that could not be unambiguously classified as belonging to any one of these categories were excluded from the present study.

One group of interneurons had cell bodies and smooth or sparsely spiny horizontal dendrites restricted to the stratum oriens. Their axon, which predominantly originated from the soma, ramified sparsely in strata radiatum and oriens and carried en passant and often drumstick-like boutons, which were distributed irregularly along them (Fig. 1*A*). Some of the axon collaterals could be followed to the subiculum or to the

20 pA). A sag (marked with arrows) indicating the presence of I_h can be seen in PCs, O-R cells and OLM cells. FS PTIs had a small or no sag. s.l-m., stratum lacunosum-moleculare; s.r., stratum radiatum; s.p., stratum pyramidale; s.o., stratum oriens.

CA3 region. The overall appearance of their axon cloud was spread out longitudinally compared to the other two interneuron types (see below). These neurons resembled a class of cells that were earlier characterised by Gulyás *et al.* (2003), Hájos *et al.* (2004) and Goldin *et al.* (2007) in slice preparations, and by Jinno *et al.* (2007) in intact brain. Although these neurons may represent a heterogeneous population of inhibitory cells including local interneurons as well as GABAergic cells with long-range projections (such as backprojecting cells, oriens retrohippocampal

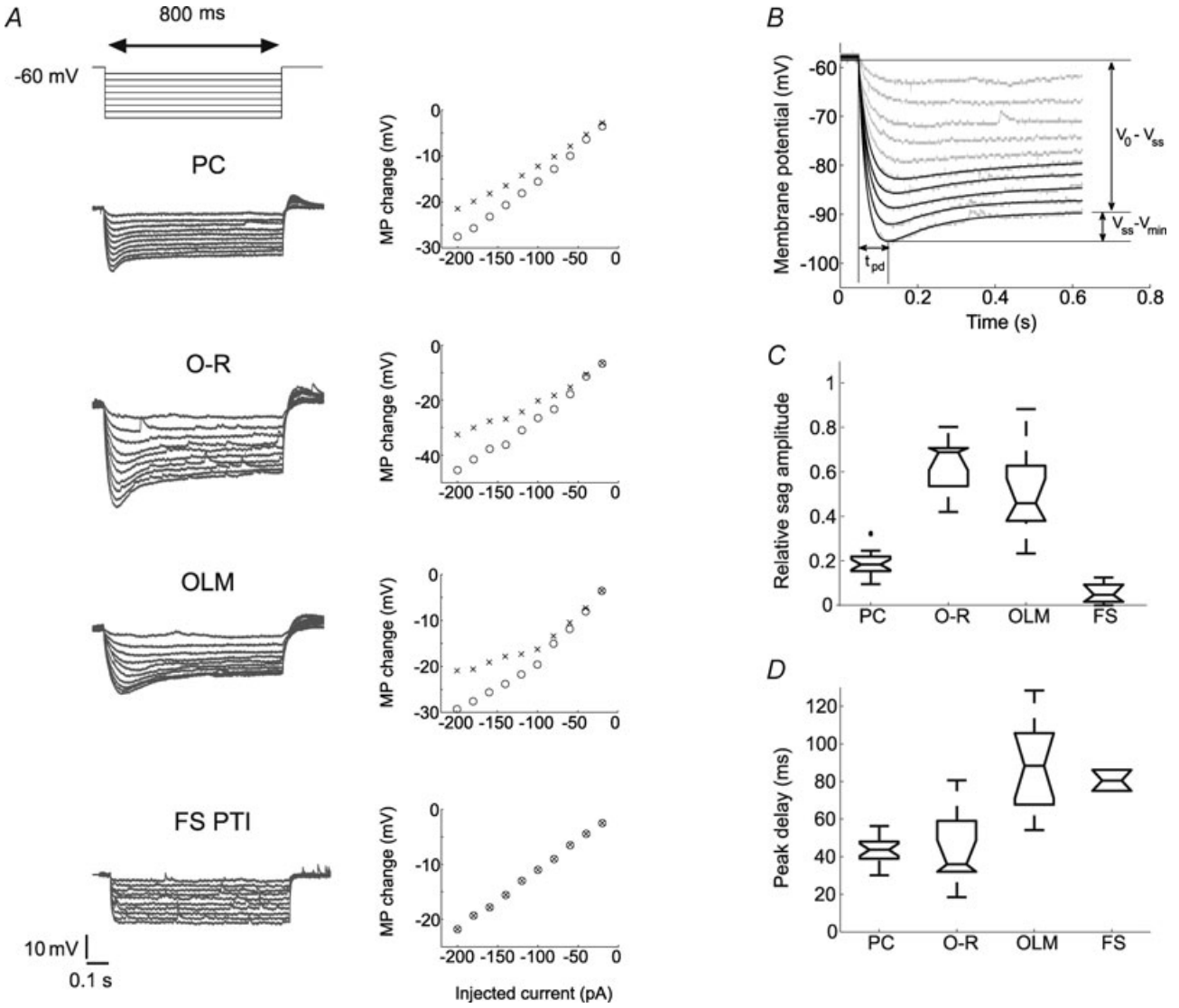

Figure 2. Properties of the sag in the investigated cell types
A, representative voltage responses of the investigated cell types to hyperpolarising current pulses (800 ms long steps from −20 to −200 pA, at 20 pA intervals from a holding potential of −60 mV), and the corresponding *I–V* plots of the peak (open circles) and the steady state membrane potential (MP) changes of the same cells (crosses). *B*, sag parameters were determined from the voltage response of the cell to the five largest amplitudes of the negative current steps (from −120 pA to −200 pA, in 20 pA steps). Relative sag amplitude is the ratio of the difference between the steady state voltage at the end of the pulse and the minimum voltage during the sag ($V_{ss} - V_{min}$), and the difference between the holding potential and the steady-state voltage ($V_o - V_{ss}$). The holding potential was approximately −60 mV in each cell. The peak delay (t_{pd}) was defined as the time of the negative peak of the membrane potential relative to the beginning of the current pulse. *C* and *D*, relative sag amplitudes and peak delays in the different cell types. Note that PCs ($n = 19$) displayed small but rather fast sag, O-R cells ($n = 11$) had a large and fast sag, while OLM cells ($n = 12$) usually showed a rather large but relatively slow sag. Two out of seven FS PTIs also showed a sag but it was rather small and could be observed only at membrane potentials negative to −90 mV.

Table 2. Properties of the impedance curves

	PC			O-R			OLM			FS PTI		
	−80	−70	−60	−80	−70	−60	−80	−70	−60	−80	−70	−60
Z	53	59	68	99	117	129	105	130	147	79	83	66
(0.5 Hz)	(43–66)	(51–80)	(60–92)	(60–128)	(76–172)	(80–154)	(98–117)	(111–148)	(135–153)	(60–93)	(69–102)	(61–105)
(MΩ)												
Q	1.17	1.22	1.14	1.10	1.12	1.05	1.10	1.05	1.04	1.02	1.01	1.00
	(1.08–1.28)	(1.14–1.32)	(1.11–1.17)	(1.04–1.35)	(1.04–1.26)	(1.04–1.24)	(1.00–1.17)	(1.00–1.15)	(1.02–1.12)	(1.00–1.04)	(1.00–1.03)	(1.00–1.02)
f_{cutoff}	18.5	16.6	13.3	14.0	11.3	9.4	7.9	6.2	4.9	18.3	14.7	20.6
(Hz)	(17.2–21.5)	(14.2–19.0)	(10.3–15.8)	(9.4–28.2)	(6.9–16.2)	(6.6–18.7)	(6.8–12.1)	(4.5–9.0)	(3.8–7.1)	(12.6–22.2)	(11.2–19.4)	(11.1–23.1)
f_{max}	5.0	6.0	5.0	2.0	2.5	2.0	1.0	1.0	1.0	1.0	0.8	1.0
(Hz)	(5.0–5.3)	(4.0–6.0)	(3.5–5.0)	(2.0–4.0)	(1.5–4.0)	(2.0–4.0)	(0.5–2.3)	(0.5–2.0)	(1.0–1.8)	(0.5–1.0)	(0.5–3.0)	(0.5–2.5)
Φ_L	0.09	0.06	0.00	0.21	0.13	0.01	0.06	0.00	0.00	0.00	0.00	0.00
(rad Hz)	(0.05–0.18)	(0.05–0.11)	(0.00–0.03)	(0.07–0.40)	(0.00–0.39)	(0.00–0.20)	(0.00–0.20)	(0.00–0.10)	(0.00–0.05)	(0.00–0.01)	(0.00–0.00)	(0.00–0.02)

Data are presented as the median with interquartile range in parentheses.

projection cells, or double projection cells based on the review of Maccaferri, 2005 and Klausberger & Somogyi, 2008), their physiological features were rather comparable; therefore the data obtained in neurons with this type of morphology were pooled under the name of oriens–radiatum (O-R) cells ($n = 24$). This name only refers to the fact that the axon collaterals of these neurons were restricted to the strata oriens and radiatum in hippocampal slices, and may not correspond to a functional category.

Another group of interneurons also had both the cell body and dendritic tree in the stratum oriens, but their horizontally running dendrites were often densely decorated with long spines. Their axon frequently originated from a proximal dendrite, and after ramification the main axon without boutons could be followed into the stratum lacunosum-moleculare. In this layer the axon ramified extensively bearing heavily packed varicosities. Some axon collaterals with boutons were also observed in the stratum oriens. These neurons were identified as oriens–lacunosum-moleculare (OLM) cells ($n = 26$) (Fig. 1*A*; McBain *et al.* 1994).

The somata of the third group of interneurons were also found in the stratum oriens, sometimes in the close vicinity of the stratum pyramidale. Their aspiny or sparsely spiny dendritic tree had either horizontal or vertical orientation, and the axonal arbour was predominantly located in the stratum pyramidale (Fig. 1*A*). Thus, these interneurons belonged to the perisomatic region-targeting inhibitory cells, which comprise both basket cells and axo-axonic cells (Freund & Buzsáki, 1996). Since the light microscopic examination of these interneurons did not allow us to unequivocally distinguish them from each other, data from all perisomatic region-targeting interneurons were pooled. Moreover, only those neurons were included in the following physiological comparison that could be classified as fast spiking cells based on the properties of their action potentials evoked by 800 ms long, 0.2 nA current pulses ($n = 7$). Therefore, we refer to them as fast-spiking perisomatic region-targeting interneurons (FS PTIs).

Basic electrophysiological characteristics

We first determined the apparent passive membrane properties (i.e. input resistance and time constant) of the neuronal classes included in our study by injecting small-amplitude hyperpolarising current steps (see Methods). Both input resistance and membrane time constant varied significantly among the different cell types (Kruskal–Wallis (KW) test, $P < 0.001$). Multiple *post hoc* comparisons (see Methods) indicated that OLM cells ($n = 12$) had a significantly higher input resistance than PCs ($P < 0.01$, $n = 19$) and FS PTIs ($P < 0.05$, $n = 7$) (Table 1). OLM cells also had a significantly slower membrane time constant at rest than any other cell type studied (OLM *vs.* PC: $P < 0.001$; OLM *vs.* O-R: $P < 0.05$; OLM *vs.* FS PTI: $P < 0.001$) (Table 1). In order to facilitate later comparisons with models that directly include capacitance as a parameter, we also estimated the membrane capacitance from the small-amplitude transient responses. Capacitance varied significantly between cell types (KW test, $P < 0.01$); in particular, OLM cells had a significantly larger capacitance than O-R cells ($n = 11$) and FS PTIs (both $P < 0.05$) (Table 1). The resting membrane potentials were estimated to be -62.4 ± 2.4 mV for PCs ($n = 21$), -55.4 ± 9.5 mV for O-R cells ($n = 17$), -55.7 ± 6.5 mV for OLM cells ($n = 19$) and -50.4 ± 8.1 mV for FS PTIs ($n = 7$) (data presented here as means ± S.D.).

Distinct features of depolarising *sag* in hippocampal neuron types

We observed a sag in the voltage response of PCs, O-R cells and OLM cells to negative current steps of suitable magnitudes (Figs 1*B* and 2*A*). In these cells a rebound depolarising hump could also be detected after the offset of the current step and in a few interneurons some rebound spikes could be observed as well (in 5 out of 17 O-R cells and in 4 out of 19 OLM cells). Both the sag and rebound depolarisation were eliminated by bath application of the specific I_h blocker, ZD7288

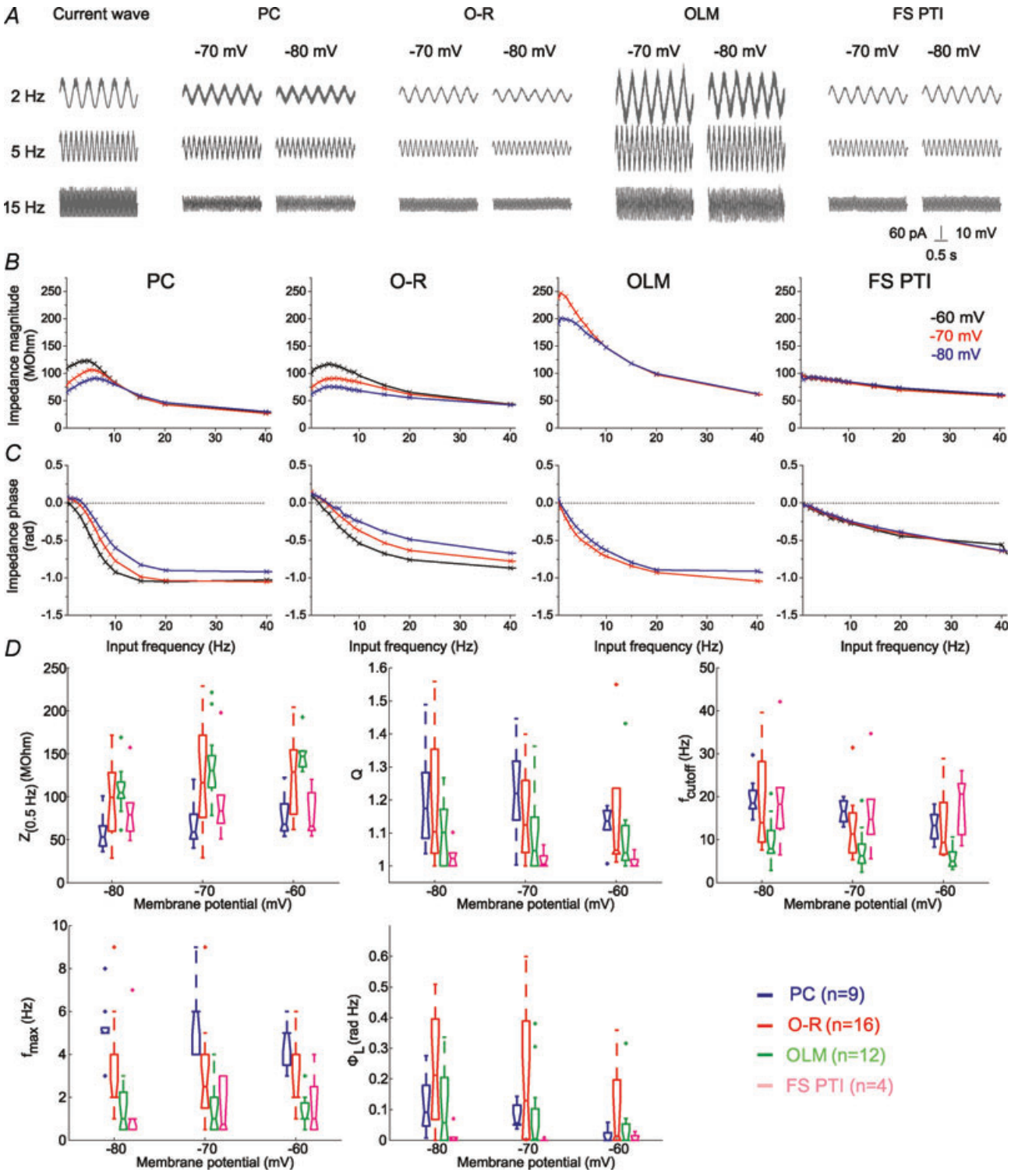

Figure 3. Characterisation of the impedance profile in the different cell types
A, voltage responses of sample cells of the investigated cell types to 3 s-long sinusoidal current inputs at 2, 5 and 15 Hz at a holding potential of −70 and −80 mV. *B*, the impedance magnitude–frequency relationship of the same cells as in *A* at different membrane potentials. PCs and O-R cells showed a clear resonance peak in the theta frequency range. Most of the OLM cells also showed resonance, although it was less apparent and occurred at lower frequencies. Fast spiking interneurons (FS PTIs) showed no subthreshold resonance. *C*, the impedance phase profile of the different cell types at the investigated potentials. Note that the amplitude and frequency extent of positive phase values increased with membrane hyperpolarisation in PCs, O-R cells and OLM cells. Colours identify corresponding membrane potentials. *D*, five parameters were used to quantitatively characterise the properties of

Table 3. Passive membrane properties and sag amplitude after the application of ZD7288

	PC ($n = 7$)	O-R ($n = 8$)	OLM ($n = 6$)	FS PTI ($n = 5$)
Input resistance (MΩ)	125 (112–159)	211 (186–235)	233 (182–245)	119 (109–190)
Membrane capacitance (pF)	220 (199–256)	160 (104–190)	208 (149–275)	135 (111–219)
Membrane time constant (ms)	25.3 (19.3–27.9)	23.5 (20.0–30.8)	26.0 (23.7–33.0)	8.9 (7.5–20.0)
Passive cutoff frequency (Hz)	6.3 (5.7–8.3)	6.8 (5.2–8.0)	6.1 (4.8–6.7)	17.9 (8.5–21.4)
Relative sag amplitude	0.066 (0.050–0.084)	0.099 (0.036–0.155)	0.076 (0.004–0.086)	0.0 (0.0–0.029)

Data are presented as median with interquartile range in parentheses.

(10 μM; data not shown). The properties of the sag varied substantially between the cell types (Fig. 2*C*,*D*). In particular, the cell types differed significantly in the relative sag amplitude ($P < 0.001$, KW test), and *post hoc* multiple comparisons indicated that O-R cells and OLM cells had a significantly larger relative sag amplitude than PCs (O-R *vs.* PC: $P < 0.001$; OLM *vs.* PC: $P < 0.01$) and FS PTIs (both $P < 0.001$) (Fig. 2*C*). The time taken to reach the negative peak amplitude of membrane potential during the current step (i.e. peak delay) also varied significantly between cell types ($P < 0.001$, KW test). OLM cells, in particular, had a significantly slower sag than PCs and O-R cells (both $P < 0.001$, *post hoc* multiple comparisons as detailed above) (Fig. 2*D*).

Qualitatively, PCs ($n = 18$ out of 19) displayed a small but rather fast sag, O-R cells ($n = 11$) had the largest and fastest sag, while OLM cells ($n = 12$) usually showed a large but relatively slow sag. In 2 out of 7 fast-spiking cells some I_h-mediated sag could be observed, but even in these particular neurons the sag was rather small and tended to appear only at very negative potentials (more negative than −90 mV).

These data suggest that, in addition to passive membrane characteristics, the properties of some active conductances such as the non-selective cation conductance mediating I_h, might be different between these cell types.

The impedance profiles and resonance properties of four types of hippocampal neuron

The differences in sag characteristics among cell types suggest that the I_h-dependent resonance could also be dissimilar. In order to characterise the subthreshold impedance profiles and possible resonance properties of the cells, a 3 s-long sinusoidal current was injected into the cells at different membrane potentials negative to the firing threshold (Fig. 3). Impedance magnitude and phase curves were characterised by five summary statistics (Table 2): impedance at 0.5 Hz ($Z_{(0.5\ \mathrm{Hz})}$; this quantity can also be used as an estimate of the input resistance of the cell, which, by definition, is the same as the impedance magnitude at 0 Hz), cutoff frequency (f_{cutoff}), resonance magnitude (Q), the frequency of maximal impedance ($f_{\max}$) and total inductive phase (Φ_L), as described in Methods. These quantities were then compared statistically between the different cell types and experimental conditions.

We found that cell type had a significant effect on all five of the derived statistics: $Z_{(0.5\ \mathrm{Hz})}$, f_{cutoff}, Q, $f_{\max}$ and Φ_L ($P < 0.001$ in each case, KW test; Fig. 3*B*–*D*). Multiple comparisons indicated that PCs had a significantly smaller $Z_{(0.5\ \mathrm{Hz})}$ than OLM cells and O-R cells (both $P < 0.001$) and FS PTIs also had a smaller $Z_{(0.5\ \mathrm{Hz})}$ than OLM cells ($P < 0.01$); f_{cutoff} was significantly lower in OLM cells than in any other cell type studied (all $P < 0.001$); Q was significantly larger in PCs, O-R cells and OLM cells than in FS PTIs ($P < 0.001$ for PCs and O-R cells, and $P < 0.05$ for OLM cells) and it was significantly larger in PCs than in OLM cells ($P < 0.01$); PCs had a significantly higher $f_{\max}$ than any other cell type (all $P < 0.001$), and $f_{\max}$ was also significantly higher in O-R cells than in OLM cells ($P < 0.01$) and FS PTIs ($P < 0.01$). Φ_L was significantly smaller in FS PTIs than in O-R cells ($P < 0.001$) and in PCs ($P < 0.05$) (Fig. 3*D*). In addition, the shape of the impedance profiles changed with variations in baseline membrane potential (Fig. 3). In particular, a two-way analysis of variance (ANOVA) using cell type as between-subject factor and membrane potential as within-subject factor showed that three of the summary statistics varied significantly with membrane potential ($Z_{(0.5\ \mathrm{Hz})}$: $P < 0.001$; f_{cutoff}: $P < 0.001$; Φ_L: $P < 0.05$).

the impedance curves. $Z_{(0.5\ \mathrm{Hz})}$ is the impedance value at the lowest input frequency (0.5 Hz). The Q value ($Z_{\max}/Z_{(0.5\ \mathrm{Hz})}$) was used to quantify the magnitude of the resonance. $f_{\max}$ means the input frequency at which the maximal impedance value was detected. Cutoff frequency (f_{cutoff}) is the input frequency where the magnitude of the impedance first dipped below $\frac{1}{\sqrt{2}} \cdot Z_{(0.5\ \mathrm{Hz})}$. Φ_L is the total inductive phase defined as the area under the positive segment of the impedance phase profile. PCs are shown in blue, O-R cells in red, OLM cells in green and FS PTIs in magenta. (See also Table 2.)

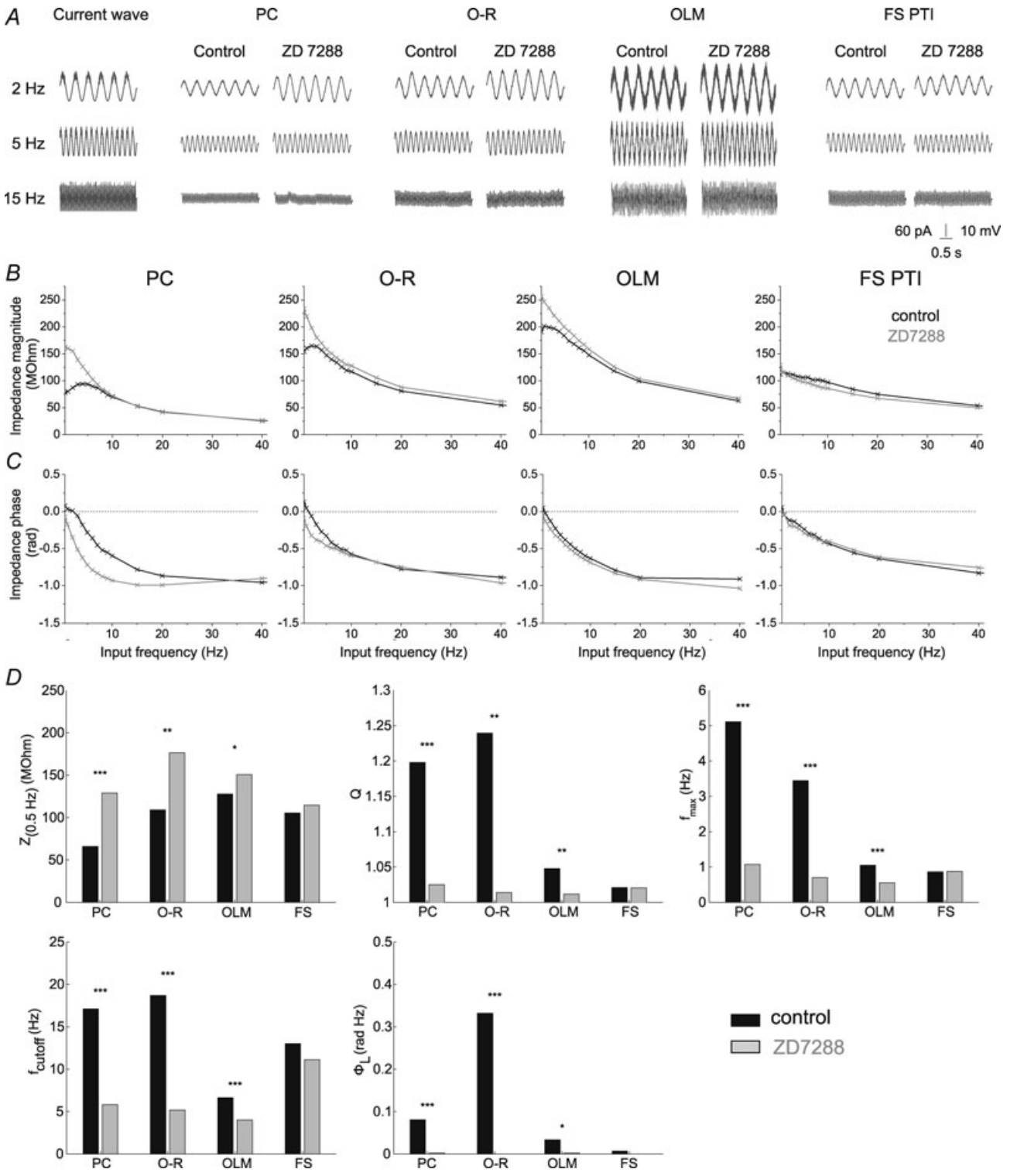

Figure 4. The effect of blocking I_h on the impedance profile of the investigated cell types
A, voltage responses of representative cells of the investigated cell types to 3 s long sinusoidal current inputs at 2, 5 and 15 Hz at a holding potential of −80 mV under control conditions and in the presence of the I_h-blocker ZD7288 (10 μM). *B* and *C*, the magnitude and phase of the impedance as a function of input frequency of the same cells measured at −80 mV in control conditions (black) and in the presence of 10 μM ZD7288 (grey). Note that after blocking I_h both the magnitude and the phase profiles changed substantially in PCs, O-R cells and OLM cells; however, ZD7288 had no apparent effect on the shape of the impedance profiles in FS PTIs. *D*, statistical comparison of the five investigated parameters in the different cell types under control

To separate cells with a monotonically decreasing impedance profile from those with resonance, resonating cells were defined as cells with a Q value greater than 1.05 at any of the investigated membrane potentials. We found that all PCs showed resonance ($n = 9$), indicated as a clear peak in the impedance curve. Resonance was most prominent at hyperpolarised potentials (at -70 and -80 mV), but was also apparent (though weaker) at depolarised potentials (Fig. 3*B* and *D*). The f_{max} values fell into the theta range (4–6 Hz) (Fig. 3*D*). Almost all O-R cells also exhibited resonance ($n = 15$ out of 16), although a rather large variance could be seen in Q values; f_{max} was between 2 and 6 Hz. Ten out of 15 OLM cells also showed resonance, but the resonance frequency fell in the range of 1–3 Hz. An obvious resonance peak could be observed in only 1 out of 7 FS PTIs at the investigated membrane potentials (Fig. 3*B* and *D*).

In line with the prediction based on the sag characteristics, both the impedance profiles and the resonance properties were found to vary substantially between the cell types. Therefore, we next investigated the contribution of I_h to their impedance profiles.

The involvement of I_h in impedance profiles and resonance

I_h is an active conductance, which was shown to be essential for the emergence of resonance behaviour in some neurons (Hutcheon *et al.* 1996*b*; Lüthi & McCormick, 1998; Hu *et al.* 2002; Narayanan & Johnston, 2007). In our experiments only those cells that showed an I_h-dependent sag showed subthreshold resonance. Furthermore, the application of 10 μM ZD7288, a blocker of HCN channels, strongly reduced or eliminated the sag in all cell types ($P < 0.001$ overall, and $P < 0.05$ in each individual cell type except FS PTIs). ZD7288 also had a moderate effect on passive membrane properties at -60 mV, increasing both the input resistance ($P < 0.05$ overall) and the apparent membrane capacitance ($P < 0.001$ overall) (Table 3). Therefore, the effect of ZD7288 on the impedance profile was tested in each of the investigated cell types. A three-way ANOVA, with cell type as a between-subject factor, and membrane potential and ZD7288 treatment as within-subject factors, indicated that ZD7288 had a significant effect on all five of our summary measures ($Z_{(0.5\ Hz)}$, f_{cutoff}, Q, f_{max}, and Φ_L; Fig. 4). In particular, the blockade of HCN channels significantly increased $Z_{(0.5\ Hz)}$ in PCs ($n = 9$, $P < 0.001$), O-R cells ($n = 6$, $P < 0.01$) and OLM cells ($n = 7$, $P < 0.01$) and significantly decreased f_{cutoff} in the same three cell types (PCs: $P < 0.001$; O-R cells: $P < 0.01$; OLM cells: $P < 0.001$). Most importantly, ZD7288 completely abolished the resonance, resulting in a significant reduction in the Q value in PCs ($P < 0.001$), O-R cells ($P < 0.01$) and in OLM cells ($P < 0.05$) (Fig. 4). The elimination of resonance by ZD7288 was also evident in the change in f_{max}, which was significant in PCs ($P < 0.001$), O-R cells ($P < 0.01$) and in OLM cells ($P < 0.01$), and in Φ_L, which was significantly reduced in the same three cell types (PCs: $P < 0.001$; O-R cells: $P < 0.01$; OLM cells: $P < 0.05$). However, ZD7288 had no effect on the shape of the impedance profile (as characterised by these five quantities) at any of the investigated membrane potentials in FS PTIs ($n = 4$) (Fig. 4).

These results suggest that I_h is essential for subthreshold resonance in pyramidal cells, O-R cells and OLM cells, and that it contributes substantially to the shape of the impedance profile even in some cells without a clear resonance, e.g. in some of the OLM cells. We also found that the shape of the impedance profile varied substantially between different cell types. Therefore, we set out to investigate whether the observed differences in the impedance curves among cell types might be due to distinct properties of I_h.

The properties of I_h in the different cell types

To examine the differences in the properties of I_h between the cell types (excluding FS PTIs since their impedance curve was not substantially affected by ZD7288 application), whole-cell voltage-clamp experiments were performed (Fig. 5*A*). First, the voltage-dependent activation of I_h was measured based on the instantaneous tail current at the end of 800 ms steps to different potentials (see Methods). We found that I_h was significantly more activated in PCs than in interneurons at all potentials between -60 and -100 mV; there was no significant difference between O-R cells and OLM cells at any membrane potential (Fig. 5*B*). Based on sigmoidal fits to activation values, the potential of half-maximal I_h activation ($V_{1/2}$) was -82.9 ± 4.9 mV in pyramidal cells ($n = 6$), -97.3 ± 4.7 mV in O-R cells ($n = 7$) and -97.7 ± 5.0 mV in OLM cells ($n = 7$, Fig. 5*B*). The slope of the activation function was similar in all cell types: the parameter m was -12.4 ± 1.9 mV in PCs,

conditions and in the presence of 10 μM ZD7288. Since ZD7288 had a similar effect at all investigated membrane potentials, data measured at different potentials were pooled in this figure. Note that ZD7288 significantly changed all properties of the impedance curves in cell types expressing a sag, but had no significant effect in FS PTIs. $^*P < 0.05$; $^{**}P < 0.01$; $^{***}P < 0.001$. (See also Table 3.)

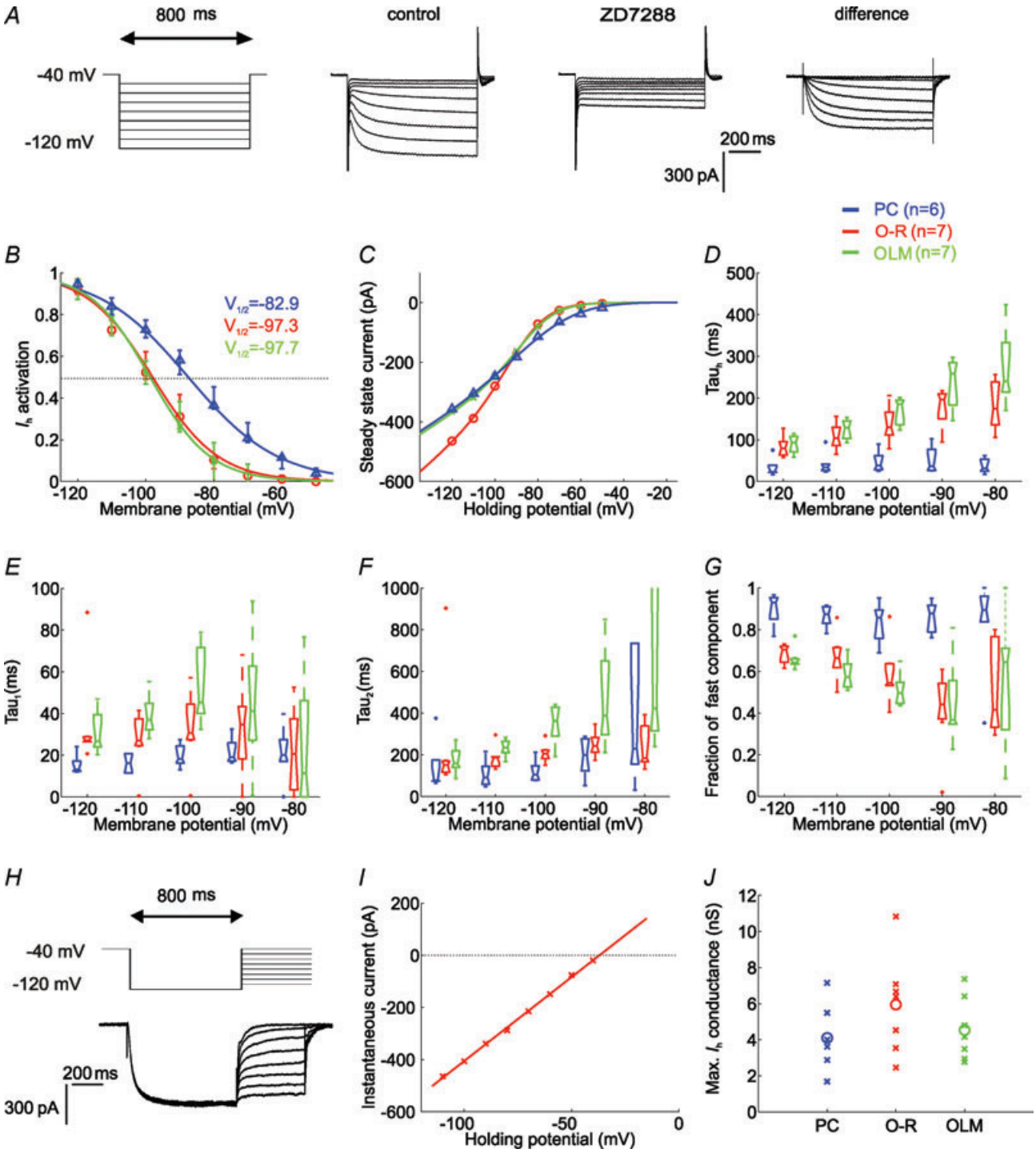

Figure 5. The properties of I_h in the different cell types
A, I_h was elicited by 800 ms-long hyperpolarising voltage steps from a holding potential of −40 mV to the range of −50 to −120 mV, in 10 mV steps. Current traces recorded before and after the application of 10 μM ZD7288. The ZD7288-sensitive current was obtained by digital subtraction. *B*, the activation curves of I_h in the investigated cell types, calculated from tail current amplitudes. *C*, the current–voltage (*I–V*) relation of I_h in the different cell types obtained by plotting steady-state currents. Note that at physiologically relevant potentials (positive to −90 mV), a significantly larger amplitude of I_h was activated in PCs than in interneurons. *D*, the activation kinetics (Tau_h) of I_h plotted against membrane potential for PCs, O-R cells and OLM cells obtained from single exponential fits. The time course of activation was generally more rapid in PCs than in interneurons over the entire voltage range. *E* and *F*, two components of the activation kinetics could be clearly identified with double exponential fits in all cell types. Fast (Tau_1, E) and slow time constant (Tau_2, F) of I_h activation as a function of voltage for PCs, O-R cells and OLM cells. In

-10.2 ± 2.7 mV in O-R cells and -8.9 ± 4.0 mV in OLM cells. No significant difference was found in the I_h reversal potential – measured using the instantaneous *I–V* plot, see Methods – between the different cell types (-33.0 ± 13.4 mV in PCs ($n = 3$), -38.8 ± 2.9 mV in O-R cells ($n = 4$), and -37.0 ± 5.9 mV in OLM cells ($n = 4$)). Therefore, reversal potential values from all cells were pooled and averaged to arrive at a single figure (-36.6 mV) that was used in all subsequent calculations and models (Fig. 5*H* and *I*). Next, we determined the maximal I_h conductance in each cell based on the steady-state current (Fig. 5*C*). We found no significant difference between the cell types, and a substantial variation within any given class (4.1 ± 1.9 nS in PCs, 5.9 ± 2.8 nS in O-R cells, and 4.6 ± 1.8 nS in OLM cells (data presented here as means $\pm$ S.D.) (Fig. 5*J*).

Finally, we analysed the kinetics of I_h by fitting either single or double exponential functions to the time course of I_h activation at different membrane potentials. Although the time course could be described fairly accurately using a single exponential function (Fig. 5*D*), a better fit was seen when a double exponential function was used, and the two components could be clearly identified in essentially all cells, with little variation within a given cell type (Fig. 5*E*,*F*). The single exponential fit indicated that activation of I_h was significantly faster at all membrane potentials between -80 and -120 mV in PCs than in O-R cells ($P < 0.001$ between -80 mV and -100 mV, and $P < 0.01$ at -110 and -120 mV) and OLM cells ($P < 0.001$ at all voltages in this range). The double exponential fit clearly identified a fast (time constant, 20–50 ms) and a slower (100–500 ms) component of I_h activation in all cell types. Both components tended to be slower in interneurons than in PCs, a difference that reached significance at some (more hyperpolarised) membrane potentials. However, the most substantial difference was in the relative weight of the two components: the activation of I_h was dominated by the fast component at all membrane potentials in PCs, while the two components contributed almost equally in interneurons (Fig. 5*G*). No significant difference was seen in the kinetics of I_h activation between O-R cells and OLM cells. The activation kinetics were found to be voltage dependent in all cell types investigated, approximated either with single or double exponential functions (Fig. 5*D–F*).

In summary, differences in the properties of I_h – specifically, the voltage dependence of steady-state activation and the kinetics of activation – between PCs and the two classes of interneuron with subthreshold resonance suggest that PCs and investigated interneuron types may express distinct subunit compositions of HCN channels, and that this may account for some of the differences in the impedance profiles between different cell types. On the other hand, the lack of any such difference in I_h characteristics between O-R cells and OLM cells, two cell types with distinct impedance profiles, indicates that factors other than the magnitude and kinetic properties of I_h are responsible for the observed variation in their impedance properties.

Computational model

To provide a quantitative account of the observed differences in the impedance profiles and resonance properties between the different cell types, we fitted the impedance profiles of single-compartment, conductance-based model neurons to those measured experimentally. The simpler model contained a membrane capacitance and a leak conductance, while the more complex model also included a voltage-gated conductance (see Methods for details). The main advantage of using models of such moderate complexity is that the impedance profile could be computed analytically by linearising the defining equations around an arbitrary baseline potential (see Methods). The relatively small number of parameters in these models also allowed us to determine, using standard non-linear optimisation algorithms, the optimal set of parameters to fit a particular set of impedance profiles (see below).

We determined and compared the best fits to individual impedance profiles using the passive model and the linearised I_h model; examples of the fits for each cell type are shown in Fig. 6*A–C* (where amplitude, phase, and

each cell type the fast time constant was about 5–8 times more rapid than the slow time constant of activation at a given potential. *G*, the fraction of the fast exponential component (Tau_1) as a function of voltage. Note that in PCs the fraction of Tau_1 was predominant over the entire voltage range, while in interneurons the fast component becomes predominant only at hyperpolarised potentials (below -100 mV) but even at -120 mV it represents only 70% of the total current amplitude. *H*, to determine the reversal potential of the current, I_h was fully activated with a voltage pulse to -120 mV and this was followed by steps to different test potentials (from -110 mV to -40 mV in 10 mV increments). *I*, the open-channel *I–V* plot was constructed from the tail current amplitudes measured at each test potential and the reversal potential of I_h was extrapolated from these plots. *J*, the estimated maximal conductance values of I_h for each cell of the different cell types (crosses). Circles indicate median values. There was no significant difference in the maximal conductance of I_h between the investigated cell types. In all plots PCs are shown in blue, O-R cells in red and OLM cells in green.

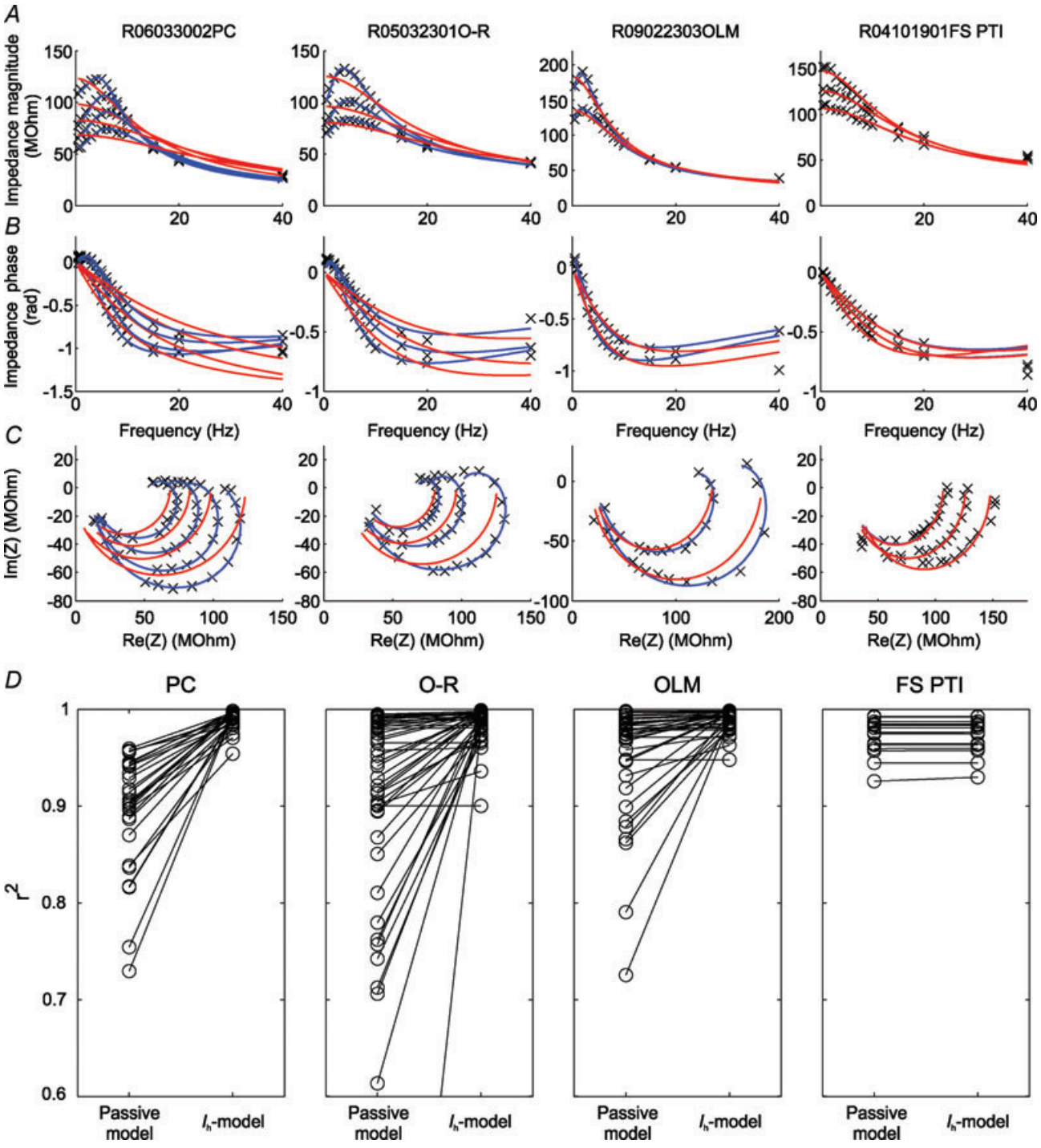

Figure 6. Comparison of fits using a passive and an active model (I_h model) in various hippocampal cell types

A–C, examples of the impedance profiles (measured at multiple membrane potentials in each cell) for a single cell of each type in the study are indicated by the crosses; the red lines show best fits to each individual curve based on a passive (three-parameter) cell model; the blue lines are best fits based on the (effectively five-parameter) I_h model (see Methods for details). *A* displays the absolute value (magnitude) of the impedance and *B* the phase of the impedance as a function of input frequency, while in *C* the complex impedance values (as defined by the magnitude and the phase) are plotted in the complex plane (in this plot, known as a Nyquist plot, frequency is not explicitly represented). *D*, comparison of fit quality between the passive and the I_h model as measured by the r-square statistic for all impedance profiles recorded under control conditions.

complex impedance are displayed separately). The passive model has only three free parameters (the input resistance, the total capacitance of the cell, and an additive serial resistance), while the linearised I_h model has five effective free parameters. (It has a total of seven parameters: the capacitance, the leak conductance, the maximal I_h conductance, the value of the activation variable at the baseline potential, the derivative of the activation variable with respect to voltage at the baseline potential, the time constant of the activation of I_h, and the series resistance, but these quantities appear only in certain combinations in the expression for the impedance, eqn (8), which reduces the number of actual free parameters to five.) We used the Bayesian information criterion (BIC, which takes into account the number of free parameters, see Methods) to compare the quality of the best fit in the two models (Fig. 6*D*). We found that the I_h model described the control impedance curves of PCs, O-R cells and OLM cells better than the passive model (median $r^2 = 0.991$ *vs.* 0.904 in PCs; $r^2 = 0.992$ *vs.* 0.949 in O-R cells; $r^2 = 0.993$ *vs.* 0.978 in OLM cells), and the value of the BIC was lower for the I_h model in these cell types, indicating that the I_h model is better even when we take into account the difference in the number of free parameters. On the other hand, the two models were about equally good at describing single control curves in FS PTIs (median $r^2 = 0.976$ for both models), and the BIC in this case favoured the passive model. In contrast, for the impedance curves measured in the presence of ZD7288, the I_h model did not perform significantly better than the passive model for any cell type (median $r^2 = 0.992$ for both models in PCs; $r^2 = 0.983$ for both models in O-R cells; $r^2 = 0.977$ *vs.* 0.976 in OLM cells; $r^2 = 0.955$ *vs.* 0.954 in FS PTIs); in fact, the simpler passive model was found to be better in all cell types according to the BIC. These results suggest that I_h makes an essential contribution to the shape of the impedance profile in PCs, O-R cells and OLM cells, converting a basically passive impedance curve into one that is more adequately described by assuming voltage-dependent mechanisms.

Next, we wanted to determine whether the presence of I_h in itself (in combination with appropriate passive characteristics) is sufficient to explain the observed impedance profiles of hippocampal neurons. We also wished to understand to what extent the observed differences in impedance curves between the different cell types could be due to differences in the properties of I_h itself, as described in the previous section. Thus, for each individual neuron, we simultaneously fitted all the available impedance curves (measured under control conditions at different baseline membrane potentials) using the linearised I_h model, with the properties of I_h (the value and the slope of the steady-state activation and the time constant, all at the appropriate membrane potentials) set according to our voltage-clamp data for the given cell type, and only four free parameters (capacitance, leak conductance and maximal I_h conductance of the neuron, and an additional series resistance) to fit for each cell. This is a much more heavily constrained fit than the ones considered above (which had 3–5 free parameters for every impedance curve, and thus up to 20 for each cell); here, the four fitted parameters are assumed to be the same at all membrane potentials in a given cell, and we constrain the voltage-gated conductance to have the cell-type-specific characteristics that we measured for I_h. Typical examples of the fit attained in different cell types are shown in Fig. 7*A*–*C* in the form of frequency–amplitude, frequency–phase, and complex (Nyquist) plots. The quality of the fit was fairly good in all cell types (median $r^2 = 0.941$ in PCs; $r^2 = 0.931$ in O-R cells; $r^2 = 0.959$ OLM cells), especially considering the small number of free parameters, indicating that I_h (in combination with passive membrane properties) is the main determinant of the subthreshold impedance profile in these cells. Importantly, the range of parameters determined through the fitting procedure (in particular, the total capacitance and the maximal I_h conductance) was in good agreement with the values measured in the experimental current-clamp and voltage-clamp protocols (Fig. 7*D*; cf. Fig. 2 and Fig. 5). Notably, our resonance fits predicted a significantly larger membrane capacitance in the OLM cell population than in the population of O-R cells ($P < 0.01$; Wilcoxon rank sum test), while there was no significant difference in the maximal conductance of I_h between the two cell types. Both of these conclusions are in agreement with our experimental measurements, and suggest that the observed differences between the impedance profiles of OLM cells and O-R cells are primarily due to a difference in passive properties rather than a difference in the kinetics or magnitude of a voltage-gated conductance (i.e. I_h).

Finally, some systematic deviations of the data from the fitted curves were also evident. These were quantified by computing for the fitted curves the five summary statistics we had defined for the characterisation of impedance profiles, and comparing them with the same statistics computed from the actual data (Fig. 7*E*). We found that the I_h model was able to capture the overall shape of the impedance profiles as measured by the input resistance and the cutoff frequency quite accurately. On the other hand, the degree of resonance (as measured by Q and Φ_{total}) and the resonant frequency were less well predicted. In particular, the fits consistently predicted a larger degree of resonance (a higher Q value) in interneurons (but not in PCs) than the value determined directly from the data. Thus, the single-compartment I_h model provides a fairly good but still incomplete account of the impedance profiles of the neurons in our study, and factors not included in this model (such as dendritic morphology, the subcellular localization of I_h, or additional voltage-gated conductances)

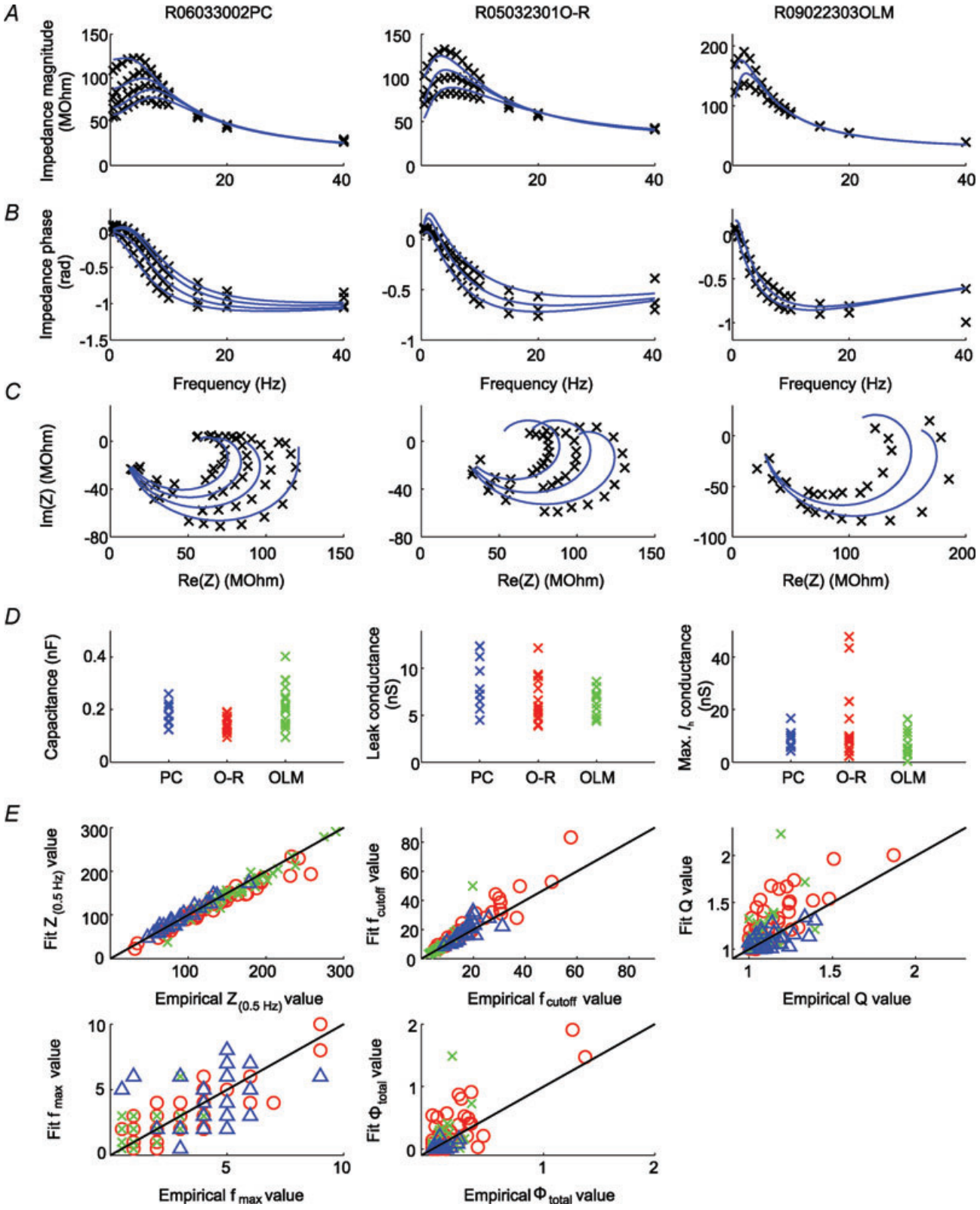

Figure 7

A–C, examples of model fits to experimentally measured impedance curves when the characteristics of I_h (voltage of half-activation, slope at half-activation, time constant) were fixed to their empirically determined values (as appropriate for each cell type), and only the capacitance, the leak conductance, and the maximal I_h conductance (as well as an additional series resistance) were allowed to vary. The types of plots in *A–C* are similar to those in

might also contribute to the measured impedance characteristics.

Discussion

Our results show that the impedance profiles of neurons calculated from their voltage responses to sinusoidal current inputs differ in pyramidal cells and different classes of interneurons investigated in the CA1 region of the hippocampus. Using electrophysiological measurements combined with computational modelling we could demonstrate that these differences arise primarily from differences in the activation properties of I_h, but the passive membrane properties of the cells also made significant contributions.

We found, in agreement with previous results, that the subthreshold resonance at theta frequencies in PCs is dependent on I_h (Hutcheon *et al.* 1996*b*; Pape & Driesang, 1998; Dickson *et al.* 2000; Hu *et al.* 2002; Fransén *et al.* 2004; Narayanan & Johnston, 2007). In addition to the I_h-mediated resonance, a so called M-resonance, produced by a depolarisation-activated potassium current below the firing threshold has also been described in PCs (Hu *et al.* 2002, 2009; Peters *et al.* 2005). According to their findings this type of resonance occurs at about −60 mV, whereas the I_h-mediated resonance they observed was only seen below −70 mV. The apparent lack of M-resonance in our experiments can be explained by the fact that we observed I_h-mediated resonance at −60 mV, suggesting that M-resonance might only be seen at more depolarised potentials, and possibly only above spike threshold under our conditions.

We found that horizontal interneurons of the stratum oriens were not uniform in their impedance properties. Although both O-R and OLM cells showed some frequency preference due to active membrane conductances, because of their high capacitance and low cutoff frequency the low-pass filter properties still dominated in OLM cells. Our results verify the earlier observations by Pike *et al.* (2000), in which some interneurons in the stratum oriens were shown to display resonance, and extend it by showing that not all oriens interneurons have the same high-pass characteristics. The finding that O-R cells and OLM cells have distinct impedance properties raises the possibility that similar synaptic input received by these two cell types (Blasco-Ibanez & Freund, 1995) may result in different discharge patterns during specific network events, such as theta and gamma rhythms or sharp-wave-associated ripple oscillations (Klausberger *et al.* 2003; Gloveli *et al.* 2005; Lawrence *et al.* 2006; Goldin *et al.* 2007; Jinno *et al.* 2007).

Previous studies (Aponte *et al.* 2006) and our observation that some FS PTIs (2 out of 7) expressed a minor sag indicate that I_h could also be present in this cell type. However, I_h does not seem to have any effect on the impedance profile of these cells at the investigated potentials. Whereas I_h-mediated subthreshold resonance was negligible in FS PTIs (present study, Hutcheon *et al.* 1996*b*), these cells exhibited obvious resonance at gamma frequencies in a study by Pike *et al.* (2000). This type of resonance is mediated by activation of persistent voltage-dependent sodium channels, opening at membrane potentials positive to −60 mV. Thus, under our conditions this form of resonance would not be expected, since we obtained recordings only at or negative to −60 mV. However, it is apparent already at these subthreshold membrane potentials that their fast membrane time constant and correspondingly high cutoff frequency would allow these cells to be capable of transmitting high frequency inputs.

Although ZD7288 is a widely used inhibitor of I_h (Harris & Constanti, 1995; Gasparini & DiFrancesco, 1997), it should be noted that ZD7288 may have unspecific effects on synaptic transmission (Chevaleyre & Castillo, 2002). However, these non-specific effects of ZD7288 were observed only after long application of the drug in rather high concentrations (∼50 μM). Thus, it seems unlikely that our results were influenced in any major way by unspecific effects of ZD7288.

Since subthreshold resonance seemed to be related to the occurrence of the membrane potential sag, which also showed significant differences among the investigated cell types, our initial supposition was that distinct resonance properties could arise from the differences in I_h properties among the different cell types. Our data revealed no significant differences between the absolute amounts of I_h-mediated conductance in the investigated cell types. However, as the observed differences in apparent membrane capacitance probably reflect differences in membrane surface area, the conductance density could still differ substantially. Although it was not possible to directly determine the conductance density from our measurements, we can estimate the cell-type dependence of this quantity by looking at the ratio

Fig. 6. *D*, values of the capacitance, the leak conductance, and the maximal I_h conductance as determined by the best fit to the measured impedance curves for each cell (with values from the three I_h-containing cell types shown separately for comparison). *E*, empirically determined summary statistics (i.e. $Z_{(0.5\ Hz)}$, f_{cutoff}, Q, f_{max}, and Φ_L) *versus* the values of the same statistics predicted by the best-fitting I_h model (with fixed I_h characteristics). Pyramidal cells are indicated by blue triangles, O-R cells by red circles, and OLM cells by green crosses.

of the measured absolute conductance and the average membrane capacitance (as estimated from current clamp experiments) in the different cell types. This comparison suggests that differences in I_h conductance density may indeed be substantial, with O-R cells having an approximately two-fold higher density than PCs and OLM cells, which may explain the stronger resonance observed in O-R cells.

Our experiments also revealed that a significantly larger amount of I_h was activated in PCs than in interneurons at physiologically relevant potentials (above −90 mV), where the resonance properties were investigated. PCs are known to express HCN channels mainly on their distal dendrites (Magee, 1998; Lörincz *et al.* 2002); therefore the differences in I_h activation might be explained by space clamp limitations. However, analysis of the activation kinetics of I_h in the distinct cell types precluded this interpretation, as more distal localization would imply slower apparent kinetics, which is opposite to our findings.

We found a clear difference in the kinetics of I_h between PCs and interneurons. Not only the time course of activation but also the relative proportion of components with a slow and a fast time constant and its change with the membrane potential were different in PCs and interneurons (Fig. 5*G*). It has been shown that the activation kinetics of HCN channels are predominantly determined by the relative contribution of HCN channel isoforms to the composition of homomeric or heteromeric channels (Santoro *et al.* 2000); therefore, one possible explanation for these differences in the activation characteristics of I_h in hippocampal neurons is different subunit compositions of HCN channels. Indeed, both immunohistochemical (Brewster *et al.* 2002; Notomi & Shigemoto, 2004) and *in situ* mRNA hybridisation studies (Santoro *et al.* 2000; Bender *et al.* 2001; Brewster *et al.* 2007) suggest that while PCs express mainly HCN1 and HCN2 in their distal dendrites, the proportion of HCN2 and HCN4 (subunits which contribute to slower activation kinetics of I_h; Franz *et al.* 2000; Santoro *et al.* 2000; Ishii *et al.* 2001) is much larger in the stratum oriens, suggesting that they are likely to be expressed in interneurons. Of course we cannot exclude the possibility that various elements of the neuronal membrane, such as putative auxiliary subunits, scaffolding proteins or cytoskeletal proteins (Wahl-Schott & Biel, 2009) interact with the HCN channels and may also influence the properties of I_h in the distinct hippocampal neurons.

In summary, the different cell types in our study were distinct both in terms of the observed properties of I_h and in terms of their passive membrane properties. The effects of various neuronal properties on the impedance profile could be predicted by the I_h model, by first using average (median) parameter values (as determined in our various experiments) for measured cell types, and then varying parameters either individually or in combination to observe the changes in the shape of the impedance curve (Fig. 8). The consequences of several manipulations are highlighted by these examples. First, changes in the half-activation voltage, which may occur in response to neuromodulatory influences (e.g. Maccaferri & McBain, 1996), essentially convert each impedance curve into one that could be measured in the original cell at a membrane potential shifted by the equivalent amount to the change in $V_{1/2}$ (but in the opposite direction). Second, alterations in the time constant of I_h profoundly affect the shape of the impedance curve, and especially the degree and frequency of resonance. Third, changes in the passive membrane resistance (the reciprocal of the leak conductance) can also have a pronounced effect on all aspects of the impedance profile, partly by changing the weight of voltage-gated conductances relative to the voltage-independent leak conductance. Fourth, the membrane capacitance affected mainly the cutoff frequency (as expected), but also played a role in shaping the resonance peak. A final important point is that no single parameter was found to be dominant in determining the differences in the characteristics of the impedance profiles of distinct cell types; concurrent changes in several parameters were required to convert one type of impedance curve into another type, as demonstrated by the last two examples in Fig. 8.

Our computational model strengthened the idea that I_h is the major determinant of the impedance characteristics at subthreshold membrane potentials in hippocampal neurons. However, our result that in stratum oriens interneurons a smaller degree of resonance was observed than that predicted from the model suggests that some other conductances might also be active at these membrane potentials in these particular cell types and dampen the effect of I_h on the impedance profile. The inward rectifier K^+ current might be a good candidate for this effect, as suggested by both theoretical and experimental studies by Hutcheon *et al.* (1996*a*,*b*) in neocortical neurons.

Physiological relevance

Several studies have shown that I_h substantially promotes firing when the fluctuation in the membrane potential can activate a sufficient number of HCN channels (Manseau *et al.* 2008). Importantly, if such fluctuation occurs simultaneously in several PCs even after the activation of a single perisomatic inhibitory cell (Cobb *et al.* 1995), then a large number of principal neurons could discharge action potentials synchronously, contributing to rhythm generation at theta frequencies. Thus, activation of I_h near or below the spike threshold might indeed be important for oscillatory activities (Kocsis & Li, 2004). This has been directly demonstrated in hippocampal slices, where blocking of I_h diminished the synchronous firing of

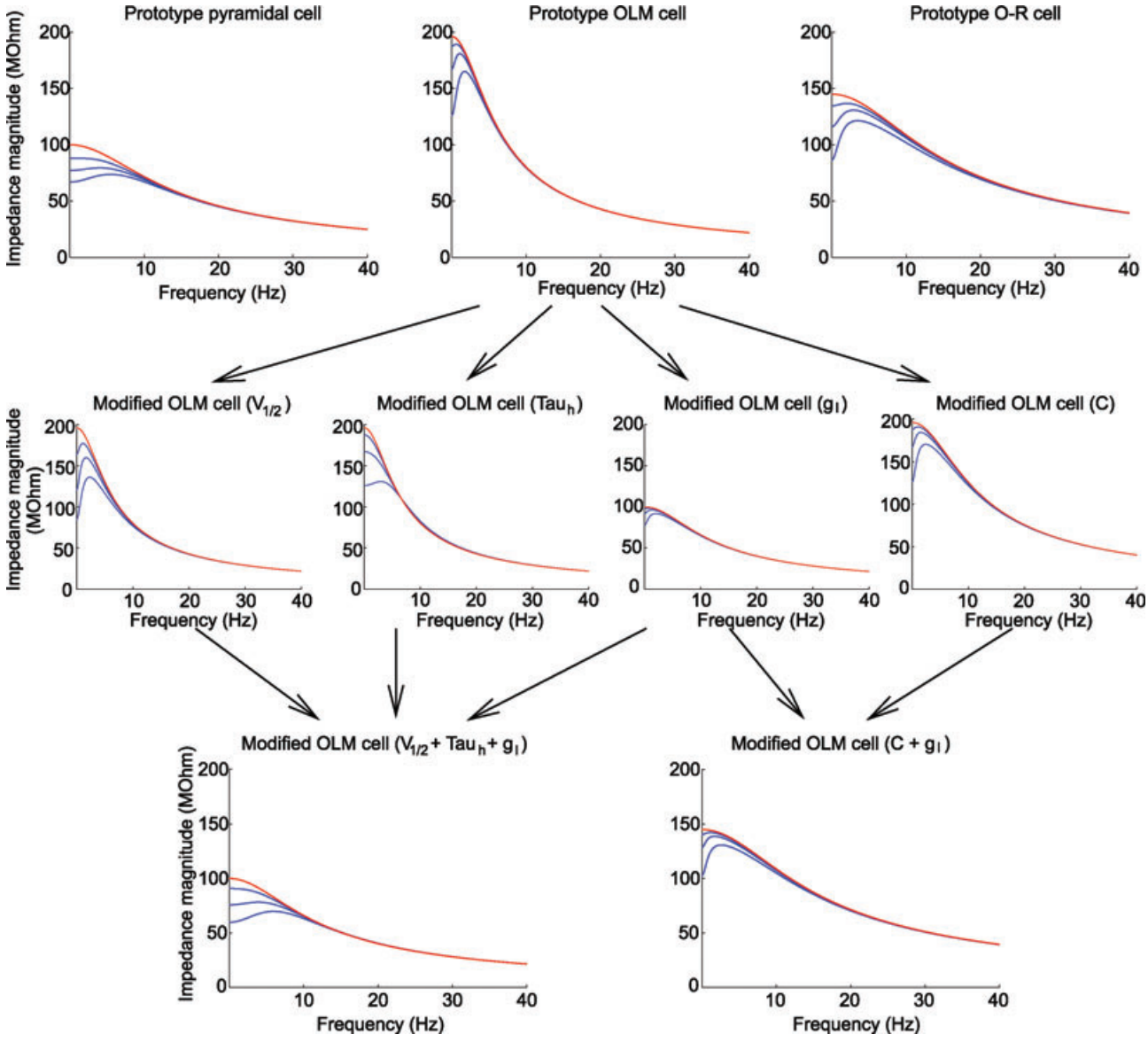

Figure 8. The effects of various cell parameters on the shape of the impedance magnitude curve
Panels in the top row show theoretically constructed impedance curves at multiple membrane potentials for the three I_h-containing cell types based on the I_h model (blue lines) using cell-type-specific median values of all parameters (g_l, C, $\bar{g}_h$, $V_{1/2}$, m, and Tau_h (V_m)) measured using current steps (Table 1) and in voltage-clamp experiments (Fig. 5).To simulate the effects of the I_h-blocker ZD7288, impedance curves were constructed using the same parameters, but with I_h set to zero (red lines). The middle row displays four theoretical examples where one of the parameters of the OLM cell model has been modified. In the first example, $V_{1/2}$ was increased by 14 mV (to −83 mV, the value characteristic of PCs) to shift the I_h activation curve to the right; in the second, Tau_h was adjusted (at all membrane potentials) to values measured for PCs, making the activation of I_h substantially faster; in the third, g_l was increased by approximately a factor of 2, thereby reducing R_{in} to a value typical of PCs; and in the fourth, C was reduced by approximately a factor of 2 to a value characterising O-R neurons. In the bottom left plot, three of these manipulations were applied simultaneously (as indicated by the arrows), resulting in impedance magnitude curves which are remarkably similar to the PC curves in the top row, despite the remaining differences in C, $\bar{g}_h$, and m. Similarly, two types of manipulation in the middle row were combined to yield the impedance curve in the bottom right, which resembles the O-R cell profile in the top row (note that the actual value of g_l in bottom right plot was different from its value in the bottom left plot, and also from the value used in the third plot in the middle row). In each plot, the blue lines represent impedance curves at three different membrane potentials (from top to bottom: −60, −70 and −80 mV) in the full I_h model, while the red curve represents a passive version of the model with $\bar{g}_h$ set to 0.

pyramidal cells at theta frequencies (Cobb *et al.* 2003). Our voltage-clamp data support these results, since a substantial proportion of HCN channels in pyramidal cells was activated at the resting membrane potential. In contrast, a much lower proportion of HCN channels would be open at resting membrane potential in OLM cells and O-R cells, which is in line with the findings that interneurons in the stratum oriens exhibited less obvious membrane potential oscillations at theta frequencies (Chapman & Lacaille, 1999).

The activation curve of I_h can be profoundly shifted by cyclic nucleotides, which are regulated by G-protein coupled receptor activation (Chen *et al.* 2001); therefore, subcortical neurotransmitter systems acting on these receptors could significantly affect the opening of HCN channels. Thus, theta frequency membrane potential oscillations as well as the impedance of the interneurons that express HCN channels can be modulated in a state-dependent manner (Fig. 8; Maccaferri & McBain, 1996; Gasparini & DiFrancesco, 1999; Placantonakis *et al.* 2000; Bickmeyer *et al.* 2002; Rosenkranz & Johnston, 2006), controlling their recruitment into network activity.

I_h has been shown to influence the occurrence of dendritic spikes (Tsay *et al.* 2007) and the amplitude of EPSPs (George *et al.* 2009) by interacting with other voltage-gated ion channels, such as N- or T-type Ca^{2+} channels or the so-called M-current mediated by voltage-gated K^+ channels. Therefore the observation that I_h is activated at more hyperpolarised potentials in oriens interneurons than in pyramidal cells might also be important in understanding the differences in dendritic signal-processing mechanisms of these cells.

While several studies have measured the impedance amplitude in various cell types, much less has been known about the phase of the impedance. We determined and compared the impedance phase profiles of four types of hippocampal neuron. In the three 'resonant' cell types in our study, positive as well as negative phase shifts could be seen depending on the frequency. Since I_h works effectively as an inductive element in the membrane, it can produce a significant positive phase shift in the voltage response of the cell to an oscillatory input. Both theoretical and experimental studies suggest that this feature of I_h might be important in many processes including control of spike timing (Lengyel *et al.* 2005; Kwag & Paulsen, 2009) and synaptic plasticity (Narayanan & Johnston, 2007, 2008). Specifically, during oscillations, the phase of the impedance quantifies the phase shift of the cell's membrane potential oscillation relative to the phase of its rhythmic current input. A positive phase shift is especially interesting, since it leads to an apparent paradox whereby the cell's response seems to lead the corresponding change in its input – although this holds in a rigorous sense only for regular sinusoidal oscillations. The fact that distinct classes of hippocampal cells show well-defined, cell-type-specific impedance amplitude and phase-response characteristics may indicate a crucial role of these cellular properties in the complex dynamics involved in information processing in the central nervous system.

References

Aponte Y, Lien CC, Reisinger E & Jonas P (2006). Hyperpolarization-activated cation channels in fast-spiking interneurons of rat hippocampus. *J Physiol* **574**, 229–243.

Bender RA, Brewster A, Santoro B, Ludwig A, Hofmann F, Biel M & Baram TZ (2001). Differential and age-dependent expression of hyperpolarization-activated, cyclic nucleotide-gated cation channel isoforms 1–4 suggests evolving roles in the developing rat hippocampus. *Neuroscience* **106**, 689–698.

Bickmeyer U, Heine M, Manzke T & Richter DW (2002). Differential modulation of I_h by 5-HT receptors in mouse CA1 hippocampal neurons. *Eur J Neurosci* **16**, 209–218.

Bishop CM (2006). *Pattern Recognition and Machine Learning*. Springer, Singapore.

Blasco-Ibanez JM & Freund TF (1995). Synaptic input of horizontal interneurons in stratum oriens of the hippocampal CA1 subfield: structural basis of feed-back activation. *Eur J Neurosci* **7**, 2170–2180.

Brewster A, Bender RA, Chen Y, Dube C, Eghbal-Ahmadi M & Baram TZ (2002). Developmental febrile seizures modulate hippocampal gene expression of hyperpolarization-activated channels in an isoform- and cell-specific manner. *J Neurosci* **22**, 4591–4599.

Brewster AL, Chen Y, Bender RA, Yeh A, Shigemoto R & Baram TZ (2007). Quantitative analysis and subcellular distribution of mRNA and protein expression of the hyperpolarization-activated cyclic nucleotide-gated channels throughout development in rat hippocampus. *Cereb Cortex* **17**, 702–712.

Chapman CA & Lacaille JC (1999). Intrinsic theta-frequency membrane potential oscillations in hippocampal CA1 interneurons of stratum lacunosum-moleculare. *J Neurophysiol* **81**, 1296–1307.

Chen S, Wang J & Siegelbaum SA (2001). Properties of hyperpolarization-activated pacemaker current defined by coassembly of HCN1 and HCN2 subunits and basal modulation by cyclic nucleotide. *J Gen Physiol* **117**, 491–504.

Chevaleyre V & Castillo PE (2002). Assessing the role of Ih channels in synaptic transmission and mossy fibre LTP. *Proc Natl Acad Sci U S A* **99**, 9538–9543.

Cobb SR, Buhl EH, Halasy K, Paulsen O & Somogyi P (1995). Synchronization of neuronal activity in hippocampus by individual GABAergic interneurons. *Nature* **378**, 75–78.

Cobb SR, Larkman PM, Bulters DO, Oliver L, Gill CH & Davies CH (2003). Activation of I_h is necessary for patterning of mGluR and mAChR induced network activity in the hippocampal CA3 region. *Neuropharmacology* **44**, 293–303.

Dickson CT, Magistretti J, Shalinsky MH, Fransén E, Hasselmo ME & Alonso A (2000). Properties and role of I_h in the pacing of subthreshold oscillations in entorhinal cortex layer II neurons. *J Neurophysiol* **83**, 2562–2579.

Drummond GB (2009). Reporting ethical matters in *The Journal of Physiology*: standards and advice. *J Physiol* **587**, 713–719.

Fransén E, Alonso AA, Dickson CT, Magistretti J & Hasselmo ME (2004). Ionic mechanisms in the generation of subthreshold oscillations and action potential clustering in entorhinal layer II stellate neurons. *Hippocampus* **14**, 368–384.

Franz O, Liss B, Neu A & Roeper J (2000). Single-cell mRNA expression of *HCN1* correlates with a fast gating phenotype of hyperpolarization-activated cyclic nucleotide-gated ion channels (I_h) in central neurons. *Eur J Neurosci* **12**, 2685–2693.

Freund TF & Buzsáki G (1996). Interneurons of the hippocampus. *Hippocampus* **6**, 345–470.

Gasparini S & DiFrancesco D (1997). Action of the hyperpolarization-activated current (I_h) blocker ZD 7288 in hippocampal CA1 neurons. *Pflugers Arch* **435**, 99–106.

Gasparini S & DiFrancesco D (1999). Action of serotonin on the hyperpolarization-activated cation current (I_h) in rat CA1 hippocampal neurons. *Eur J Neurosci* **11**, 3093–3100.

George MS, Abbott LF & Siegelbaum SA (2009). HCN hyperpolarization-activated cation channels inhibit EPSPs by interactions with M-type K^+ channels. *Nat Neurosci* **12**, 577–584.

Gloveli T, Dugladze T, Saha S, Monyer H, Heinemann U, Traub RD, Whittington MA & Buhl EH (2005). Differential involvement of oriens/pyramidale interneurones in hippocampal network oscillations in vitro. *J Physiol* **562**, 131–147.

Goldin M, Epsztein J, Jorquera I, Represa A, Ben-Ari Y, Crepel V & Cossart R (2007). Synaptic kainate receptors tune oriens-lacunosum moleculare interneurons to operate at theta frequency. *J Neurosci* **27**, 9560–9572.

Gulyás AI, Miles R, Hájos N & Freund TF (1993). Precision and variability in postsynaptic target selection of inhibitory cells in the hippocampal CA3 region. *Eur J Neurosci* **5**, 1729–1751.

Gulyás AI, Hájos N, Katona I & Freund TF (2003). Interneurons are the local targets of hippocampal inhibitory cells which project to the medial septum. *Eur J Neurosci* **17**, 1861–1872.

Hájos N, Pálhalmi J, Mann EO, Németh B, Paulsen O & Freund TF (2004). Spike timing of distinct types of GABAergic interneuron during hippocampal gamma oscillations in vitro. *J Neurosci* **24**, 9127–9137.

Han ZS (1994). Electrophysiological and morphological differentiation of chandelier and basket cells in the rat hippocampal formation: a study combining intracellular recording and intracellular staining with biocytin. *Neurosci Res* **19**, 101–110.

Harris NC & Constanti A (1995). Mechanism of block by ZD 7288 of the hyperpolarization-activated inward rectifying current in guinea pig substantia nigra neurons in vitro. *J Neurophysiol* **74**, 2366–2378.

Hu H, Vervaeke K & Storm JF (2002). Two forms of electrical resonance at theta frequencies, generated by M-current, h-current and persistent Na^+-current in rat hippocampal pyramidal cells. *J Physiol* **545**, 783–805.

Hu H, Vervaeke K, Graham LJ & Storm JF (2009). Complementary theta resonance filtering by two spatially segregated mechanisms in CA1 hippocampal pyramidal neurons. *J Neurosci* **29**, 14472–14483.

Hutcheon B, Miura RM, Yarom Y & Puil E (1994). Low-threshold calcium current and resonance in thalamic neurons: a model of frequency preference. *J Neurophysiol* **71**, 583–594.

Hutcheon B, Miura RM & Puil E (1996*a*). Models of subthreshold membrane resonance in neocortical neurons. *J Neurophysiol* **76**, 698–714.

Hutcheon B, Miura RM & Puil E (1996*b*). Subthreshold membrane resonance in neocortical neurons. *J Neurophysiol* **76**, 683–697.

Hutcheon B & Yarom Y (2000). Resonance, oscillation and the intrinsic frequency preferences of neurons. *Trends Neurosci* **23**, 216–222.

Ishii TM, Takano M & Ohmori H (2001). Determinants of activation kinetics in mammalian hyperpolarization-activated cation channels. *J Physiol* **537**, 93–100.

Jinno S, Klausberger T, Marton LF, Dalezios Y, Roberts JD, Fuentealba P, Bushong EA, Henze D, Buzsáki G & Somogyi P (2007). Neuronal diversity in GABAergic long-range projections from the hippocampus. *J Neurosci* **27**, 8790–8804.

Kamondi A, Acsády L, Wang XJ & Buzsáki G (1998). Theta oscillations in somata and dendrites of hippocampal pyramidal cells in vivo: activity-dependent phase-precession of action potentials. *Hippocampus* **8**, 244–261.

Klausberger T, Magill PJ, Marton LF, Roberts JD, Cobden PM, Buzsaki G & Somogyi P (2003). Brain-state- and cell-type-specific firing of hippocampal interneurons in vivo. *Nature* **421**, 844–848.

Klausberger T & Somogyi P (2008). Neuronal diversity and temporal dynamics: the unity of hippocampal circuit operations. *Science* **321**, 53–57.

Kocsis B & Li S (2004). In vivo contribution of h-channels in the septal pacemaker to theta rhythm generation. *Eur J Neurosci* **20**, 2149–2158.

Kwag J & Paulsen O (2009). The timing of external input controls the sign of plasticity at local synapses. *Nat Neurosci* **12**, 1219–1221.

Lawrence JJ, Grinspan ZM, Statland JM & McBain CJ (2006). Muscarinic receptor activation tunes mouse stratum oriens interneurones to amplify spike reliability. *J Physiol* **571**, 555–562.

Lengyel M, Kwag J, Paulsen O & Dayan P (2005). Matching storage and recall: hippocampal spike timing-dependent plasticity and phase response curves. *Nat Neurosci* **8**, 1677–1683.

Leung LS & Yu HW (1998). Theta-frequency resonance in hippocampal CA1 neurons in vitro demonstrated by sinusoidal current injection. *J Neurophysiol* **79**, 1592–1596.

Lien CC & Jonas P (2003). Kv3 potassium conductance is necessary and kinetically optimized for high-frequency action potential generation in hippocampal interneurons. *J Neurosci* **23**, 2058–2068.

Lörincz A, Notomi T, Tamás G, Shigemoto R & Nusser Z (2002). Polarized and compartment-dependent distribution of HCN1 in pyramidal cell dendrites. *Nat Neurosci* **5**, 1185–1193.

Lüthi A & McCormick DA (1998). H-current: properties of a neuronal and network pacemaker. *Neuron* **21**, 9–12.

Maccaferri G & McBain CJ (1996). The hyperpolarization-activated current (I_h) and its contribution to pacemaker activity in rat CA1 hippocampal stratum oriens-alveus interneurones. *J Physiol* **497**, 119–130.

Maccaferri G (2005). Stratum oriens horizontal interneurone diversity and hippocampal network dynamics. *J Physiol* **562**, 73–80.

Magee JC (1998). Dendritic hyperpolarization-activated currents modify the integrative properties of hippocampal CA1 pyramidal neurons. *J Neurosci* **18**, 7613–7624.

Magee JC (1999). Dendritic I_h normalizes temporal summation in hippocampal CA1 neurons. *Nat Neurosci* **2**, 508–514.

Manseau F, Goutagny R, Danik M & Williams S (2008). The hippocamposeptal pathway generates rhythmic firing of GABAergic neurons in the medial septum and diagonal bands: an investigation using a complete septohippocampal preparation in vitro. *J Neurosci* **28**, 4096–4107.

McBain CJ, DiChiara TJ & Kauer JA (1994). Activation of metabotropic glutamate receptors differentially affects two classes of hippocampal interneurons and potentiates excitatory synaptic transmission. *J Neurosci* **14**, 4433–4445.

McLelland D & Paulsen O (2009). Neuronal oscillations and the rate-to-phase transform: mechanism, model and mutual information. *J Physiol* **587**, 769–785.

Narayanan R & Johnston D (2007). Long-term potentiation in rat hippocampal neurons is accompanied by spatially widespread changes in intrinsic oscillatory dynamics and excitability. *Neuron* **56**, 1061–1075.

Narayanan R & Johnston D (2008). The h channel mediates location dependence and plasticity of intrinsic phase response in rat hippocampal neurons. *J Neurosci* **28**, 5846–5860.

Nolan MF, Malleret G, Lee KH, Gibbs E, Dudman JT, Santoro B, Yin D, Thompson RF, Siegelbaum SA, Kandel ER & Morozov A (2003). The hyperpolarization-activated HCN1 channel is important for motor learning and neuronal integration by cerebellar Purkinje cells. *Cell* **115**, 551–564.

Notomi T & Shigemoto R (2004). Immunohistochemical localization of I_h channel subunits, HCN1–4, in the rat brain. *J Comp Neurol* **471**, 241–276.

Pape HC & Driesang RB (1998). Ionic mechanisms of intrinsic oscillations in neurons of the basolateral amygdaloid complex. *J Neurophysiol* **79**, 217–226.

Pawelzik H, Hughes DI & Thomson AM (2002). Physiological and morphological diversity of immunocytochemically defined parvalbumin- and cholecystokinin-positive interneurones in CA1 of the adult rat hippocampus. *J Comp Neurol* **443**, 346–367.

Peters HC, Hu H, Pongs O, Storm JF & Isbrandt D (2005). Conditional transgenic suppression of M channels in mouse brain reveals functions in neuronal excitability, resonance and behaviour. *Nat Neurosci* **8**, 51–60.

Pike FG, Goddard RS, Suckling JM, Ganter P, Kasthuri N & Paulsen O (2000). Distinct frequency preferences of different types of rat hippocampal neurones in response to oscillatory input currents. *J Physiol* **529**, 205–213.

Placantonakis DG, Schwarz C & Welsh JP (2000). Serotonin suppresses subthreshold and suprathreshold oscillatory activity of rat inferior olivary neurones in vitro. *J Physiol* **524**, 833–851.

Richardson MJ, Brunel N & Hakim V (2003). From subthreshold to firing-rate resonance. *J Neurophysiol* **89**, 2538–2554.

Rosenkranz JA & Johnston D (2006). Dopaminergic regulation of neuronal excitability through modulation of I_h in layer V entorhinal cortex. *J Neurosci* **26**, 3229–3244.

Santoro B, Chen S, Lüthi A, Pavlidis P, Shumyatsky GP, Tibbs GR & Siegelbaum SA (2000). Molecular and functional heterogeneity of hyperpolarization-activated pacemaker channels in the mouse CNS. *J Neurosci* **20**, 5264–5275.

Tsay D, Dudman JT & Siegelbaum SA (2007). HCN1 channels constrain synaptically evoked Ca^{2+} spikes in distal dendrites of CA1 pyramidal neurons. *Neuron* **56**, 1076–1089.

Wahl-Schott C & Biel M (2009). HCN channels: structure, cellular regulation and physiological function. *Cell Mol Life Sci* **66**, 470–494.

Ylinen A, Soltész I, Bragin A, Penttonen M, Sík A & Buzsáki G (1995). Intracellular correlates of hippocampal theta rhythm in identified pyramidal cells, granule cells, and basket cells. *Hippocampus* **5**, 78–90.

Author contributions

R.Z., S.K., O.P. and N.H. contributed to the conception and design of the experiments. R.Z. conducted the electrophysiological experiments. S.K. performed the modelling part of the study. R.Z. and S.K. analysed the data. R.Z., S.K., O.P., T.F.F. and N.H. participated in the interpretation of the data. All authors drafted the manuscript and approved the final version for publication. Experiments were conducted in the Department of Cellular and Network Neurobiology, Institute of Experimental Medicine, Hungarian Academy of Sciences, Budapest, Hungary.

Acknowledgements

We thank Ms Katalin Lengyel and Erzsébet Gregori for their excellent technical assistance. This work was supported by the Hungarian Scientific Research Fund (OTKA T049517, OTKA K60927, NKTH-OTKA CNK 77793), the Wellcome Trust, the BBSRC, and the British Council.